



1       **Characterization of ambient volatile organic compounds, source**  
2       **apportionment, and the ozone-NO<sub>x</sub>-VOC sensitivities in a heavily**  
3       **polluted megacity of central China: Effect of sporting events and the**  
4       **emission reductions**

5       Shijie Yu<sup>a,b,1</sup>, Fangcheng Su<sup>a,b,1</sup>, Shasha Yin<sup>b,c</sup>, Shenbo Wang<sup>a,b</sup>, Ruixin Xu<sup>b,c</sup>, Bing He<sup>d</sup>,  
6       Xiangge Fan<sup>d</sup>, Minghao Yuan<sup>d</sup>, Ruiqin Zhang<sup>b,c\*</sup>

7       *a. College of Chemistry, Zhengzhou University, Zhengzhou 450001, China*

8       *b. Institute of Environmental Sciences, Zhengzhou University, Zhengzhou 450001,*  
9       *China*

10      *c. School of Ecology and Environment, Zhengzhou University, Zhengzhou, 450001,*  
11      *China*

12      *d. Environmental Protection Monitoring Center Station of Zhengzhou, Zhengzhou*  
13      *450007, China*

14

15

16

17

18

19       \*Correspondence author. Research Institute of Environmental Science, College  
20       of Environment and Ecology, Zhengzhou University High-tech Development Zone,  
21       Zhengzhou, Henan, PR China, 450001

22       E-mail address: [rqzhang@zzu.edu.cn](mailto:rqzhang@zzu.edu.cn)

23       <sup>1</sup> These authors contributed equally to this work.

24



25           **Abstract:** The implementation of strict emission control during the 11th National  
26 Minority Games (NMG) in September 2019 provided a valuable opportunity to assess  
27 the impact of such emission controls on the characteristics of VOCs and other air  
28 pollutants. Here, we investigated the characteristics of VOCs and the O<sub>3</sub>-NO<sub>x</sub>-VOCs  
29 sensitivity comprehensively in Zhengzhou before, during, and after the NMG by  
30 delivering field measurements combined with the WRF (Weather Research and  
31 Forecasting)-CMAQ (Community Multi-scale Air Quality) model simulations. The  
32 average mixing ratios of VOCs during the control periods were 34 ppbv, and cut down  
33 by about 16% before and after emission reduction. The ozone precursors (NO<sub>x</sub>) also  
34 decreased significantly during the control period; however, the ozone pollution was  
35 severe during the entire observation period. Positive Matrix Factorization analysis  
36 indicated seven major sources of ambient VOCs, including coal combustion, biomass  
37 burning, vehicle exhausts, industrial processes, biogenic emissions, solvent utilization  
38 and liquefied petroleum gas (LPG). The results show that the major source emissions,  
39 such as coal combustion and solvent utilization, were significantly reduced during the  
40 control period. As for ozone formation potential (OFP), the value during the control  
41 period was 183 μg/m<sup>3</sup>, which was 0.23 and 0.17 times lower than those before and  
42 after control period, respectively. Solvent utilization and combustion controls were  
43 the most important measures taken to reduce OFP during NMG period. Through  
44 control policies, it can effectively reduce carcinogenic risk. However, non-cancer  
45 risks of ambient VOC exposures were all exceeding the safe level (hazard quotient =  
46 1) during the sampling periods, and emphasis on the reduction of acrolein emissions



47 was needed. In addition, the WRF/CMAQ model simulation indicated that O<sub>3</sub>  
48 formation was controlled by VOCs in Zhengzhou. The results of the Empirical  
49 Kinetic Modelling Approach showed that the NO<sub>x</sub> reduction in Zhengzhou might led  
50 to higher ozone pollution. It is suggested that reduction ratios of the precursors  
51 (VOCs:NO<sub>x</sub>) is more than 2, which can effectively alleviate ozone pollution.

52 **Keywords:** Volatile organic compounds; the National Minority Games; Emission  
53 control; Empirical Kinetic Modeling Approach (EKMA); Health risk assessment.

54



## 55 1. Introduction

56 Volatile organic compounds (VOCs), important precursors for the generation of  
57 near-surface ozone (O<sub>3</sub>) and secondary organic aerosols (SOA), have received  
58 widespread attention in the world (Baudic et al., 2016; Xiong and Du, 2020; Yadav et  
59 al., 2019; Yang et al., 2019a; Zeng et al., 2018; Zhang et al., 2015). Moreover, VOCs  
60 have adverse impacts on human health, which induce cancer directly and  
61 associate with increased long-term health risks (Hu et al., 2018; Jaars et al., 2018).  
62 Since the beginning of the 21st Century, heavy air pollution event has frequently  
63 occurred in China, characterized by regional and complex air pollution (Li et al.,  
64 2019d; Ma et al., 2019). Therefore, the improvement of air quality has become a hot  
65 issue, especially for large-scale activities held in megacities, and how to ensure air  
66 quality becomes the key to the success of the activities.

67 Air quality assurance refers to the systematic emission reduction and control  
68 measures of pollution sources to ensure air quality during special activities.  
69 Temporarily enhanced control measures could provide a scenario to analyze the  
70 response relationship between emission sources of pollutants and ambient air quality.  
71 Many scholars have carried out researches on pollutant characteristics and their  
72 source apportionment under different control measures for a variety of special  
73 activities. Those studies included the 2008 Beijing Olympic Games (Schleicher et al.,  
74 2012; Wang et al., 2009), the 2010 World Expo in Shanghai (Chan et al., 2015; Wang  
75 et al., 2014), the 2014 Asia-Pacific Economic Cooperation Summit in Beijing (Li et



76 al., 2015, 2017), 70th China Victory Day Parade anniversary (Huang et al., 2018; Ren  
77 et al., 2019) and the G20 summit in Hangzhou (Li et al., 2019b; Zhang et al., 2020).  
78 These studies all suggested that enhanced emission-reduction strategies had  
79 significant effects on improving air quality. O<sub>3</sub> pollution might not be improved and  
80 even worsen during the control period (Xu et al., 2019). The relationship between O<sub>3</sub>  
81 and its precursors is nonlinear, and unreasonable reduction of O<sub>3</sub> precursors might not  
82 necessarily alleviate O<sub>3</sub> pollution. Hence, it is necessary to investigate an in-depth  
83 understanding of the mechanism involved in O<sub>3</sub> formation, especially under the  
84 emission reduction scenario. However, studies on these special events have mostly  
85 focused on particulate matter and its components, and to a much lesser degree on  
86 ozone and VOCs. In particular, the discussion on O<sub>3</sub> sensitivity and implications for  
87 control strategies through the combination of model and observation-based methods is  
88 still lacking. Furthermore, these studies mainly focused on few metropolises in China,  
89 especially in the three most developed regions, Beijing-Tianjin-Hebei (BTH) region,  
90 Yangtze River Delta (YRD) region and Pearl River Delta (PRD) region.

91 From 8<sup>th</sup> -16<sup>th</sup> September , 2019, the 11th National Minority Games (NMG) was  
92 held in Zhengzhou, China. As the host city, Zhengzhou took emergency pollution  
93 control measures in the city and neighboring regions from 26<sup>th</sup> August to 18<sup>th</sup>  
94 September for enhancing air quality during NMG period. Considering that the ozone  
95 pollution is the main pollution in the region in September (Yu et al., 2020),  
96 Zhengzhou municipal government has focused on the emission reduction of VOCs  
97 and NO<sub>x</sub> to alleviate O<sub>3</sub> pollution. Based on the bottom-up emission inventories and



98 observation-based source apportionment, major anthropogenic sources of VOCs in the  
99 area include vehicular exhaust, liquefied petroleum gas (LPG) evaporation, solvent  
100 usage and industrial emissions (Bai et al., 2020; Li et al., 2019a). Thus, they are the  
101 target emission sources when temporary invention measures are adopted for  
102 controlling air pollution during NMG period. A detailed description of the control  
103 measures is shown in Table S1. It is an excellent opportunity to determine the effects  
104 of emission control policies by using the real atmosphere as a natural laboratory.  
105 Therefore, it is necessary to investigate VOC characteristics and sources, as well as  
106 their effects on ozone production before, during, and after the control period.

107 This study measured 106 VOC species using on-line gas chromatography-mass  
108 spectrometry/flame ionization detector (GC-MS/FID). Meanwhile, the Weather  
109 Research and Forecasting/Community Multi-scale Air Quality (WRF/CMAQ) models  
110 were used to investigate the nonlinearity of O<sub>3</sub> response to precursor reductions. The  
111 main objectives of this study are to: (1) analyze the effects of emergent  
112 emission-reduction strategies on the VOC characteristics; (2) identify the crucial  
113 sources of VOCs in Zhengzhou and their changes during the NMG period; (3)  
114 investigate the contribution to ozone formation and risk assessment under control  
115 measures; and (4) assess the O<sub>3</sub>-NO<sub>x</sub>-VOCs sensitivity and propose control strategies  
116 for ozone episodes.



## 117 **2. Methodology**

### 118 **2.1 Site description and chemical analysis**

119 The sampling site is located on the rooftop of a four-story building at the  
120 municipal environmental monitoring station (MEM; 113.61° E, 34.75° N), about 6.6  
121 km away from the Zhengzhou Olympic Sports Center (Fig. S1). The surrounding area  
122 of the sampling site is mainly commercial and residential district, and the station is  
123 300 m west to the Qinling Road and 200 m south to the Zhongyuan Road. No  
124 significant industrial sources present around the sampling sites. The above two roads  
125 carry very heavy traffic. Accordingly, mobile source may contribute more to the VOC  
126 concentrations of the site.

127 VOC samples were collected from 6<sup>th</sup> August to 30<sup>th</sup> September, 2019, and  
128 divided into three periods, including pre-NMG period (6<sup>th</sup>-25<sup>th</sup> August), NMG period  
129 (26<sup>th</sup> August to 18<sup>th</sup> September) and after NMG (19<sup>th</sup>-30<sup>th</sup> September). By comparing  
130 the characteristics of VOC pollution during the three periods, the effects of control  
131 policies by government can clearly be identified and assessed.

132 It should be pointed out that the MEM station is located in the air monitoring  
133 network operated by Zhengzhou environmental monitoring center. The  
134 meteorological parameters (temperature, relative humidity, atmospheric pressure,  
135 wind direction and wind speed) and trace gases (O<sub>3</sub>, NO and NO<sub>x</sub>) were observed at  
136 the sampling site simultaneously. Information detailing relevant equipment was  
137 described by Li et al. (2019a)



138 Ambient VOCs were collected and analyzed continuously by using an online  
139 GC-MS/FID, and the time resolution is 1h (TH-PKU 300B, Wuhan Tianhong  
140 Instrument Co. China). This measurement was described by Li et al. (2018). Briefly,  
141 this system has two gas channels and dual detectors, in which the C<sub>2</sub>–C<sub>5</sub> non-methane  
142 hydrocarbons (NMHCs) were separated on a PLOT-Al<sub>2</sub>O<sub>3</sub> column (15 m × 0.32 mm  
143 × 6.0 μm, Dikma Technologies, Beijing, China) and quantified by FID, while the  
144 other species were separated on a DB-624 column (60 m × 0.25 mm × 1.4 μm,  
145 Agilent Technologies, Santa Clara, CA, USA) and detected by a mass  
146 selective detector with Deans switch.

147 To ensure the validity and reliability of observation data, these chemical analyses  
148 were subjected to quality assurance and quality control procedures. We used external  
149 and internal standard methods to quantify the C<sub>2</sub>–C<sub>5</sub> and C<sub>5</sub>–C<sub>12</sub> compounds  
150 respectively. Before monitoring, the standard curves of five concentrations (0.4–8  
151 ppbv) were made by using PAMS (photochemical assessment monitoring stations)  
152 standard gas, TO-15 Calibration Standards (US EPA, 1999) and four internal  
153 standard , including bromochloromethane, 1,4-difluorobenzene, chlorobenzene-d<sub>5</sub>,  
154 and bromofluorobenzene. The above standard gases and internal standard gases  
155 were provided by Apel–Riemer Environmental, USA. In addition, we input 4 ppbv  
156 PAMS+TO-15 standard gas at 0:00 local standard time (LST) every day to calibrate  
157 the data and check the stability. The coefficients of determination (R<sup>2</sup>) of calibration  
158 curves were mostly above 0.99 and the method detection limit (MDL) ranged from  
159 0.003 to 0.047 ppbv for each species. A total of 106 VOC species were detected,





160 including alkanes (29), alkenes (11), aromatics (17), halocarbons (35), Oxygenated  
161 VOCs (OVOCs) (12), acetylene, and carbon disulfide (Table S2).

## 162 **2.2 WRF-CMAQ model**

163 The WRF-CMAQ modeling system was applied to simulate ozone concentration  
164 and investigate O<sub>3</sub> sensitivity in this study. The modeling system, has been widely  
165 used for regional-scale air quality studies, and more details can be found  
166 at <http://cmascener.org/cmaq/>.

167 In this paper, the simulation period was 00:00 LST, August 5, 2019, to 23:00  
168 LST, September 30, 2019, which corresponded to the NMG sampling periods. To  
169 eliminate the impact of the initial conditions, a 5-day spin-up period was set in the  
170 simulation. We applied four-nested domain with a grid resolution of 36 × 36 km,  
171 12 × 12 km, 4 km × 4 km and 1 km × 1 km, respectively (as shown in Fig. S2). The  
172 gridded anthropogenic emission inventory by Tsinghua University was applied in  
173 CMAQ, and the local emission inventory of Henan Province was also input into the  
174 model (Bai et al., 2020). These modeling systems have been successfully used in  
175 previous simulations by Zhang et al. (2014) and Wang et al. (2019a). The results of  
176 WRF-CMAQ model evaluation in Zhangzhou were reported in our previous studies  
177 (Su et al., 2021).

## 178 **2.3 Source apportionment by PMF model**

179 PMF analysis of VOCs was performed with the USEPA PMF 5.0 program; this  
180 receptor model is widely used for source analysis. Detailed information about this



181 method is described in the user manual and related literature (Norris et al., 2014;  
182 Xiong and Du, 2020; Yenisoy-Karakas et al., 2020).

183 It must be said that not all of the VOC species were used in the PMF analysis.  
184 According to previous studies, the principles for VOC species choice were listed as  
185 following (Hui et al., 2019): (1) Species with more than 25% data missing or that fell  
186 below the MDLs were rejected; (2) Species with signal-to-noise ratio lower than 1.5  
187 were excluded.; and (3) species with represented source tracers of emission sources  
188 were retained. Eventually, a total of 42 VOC species were selected for the source  
189 apportionment analysis. In this study, a seven-factor solution was chosen in the PMF  
190 analysis based on two parameters (Ulbricht et al., 2009): (1)  $Q_{true}/Q_{robust}$  values and (2)  
191  $Q_{true}/Q_{theoretical}$  values (Fig. S3).

## 192 **2.4 Potential source contribution function (PSCF)**

193 The Potential Source Contribution Function (PSCF) is a function with  
194 conditional probability for calculating backward trajectories and identifying potential  
195 source regions. The detailed descriptions of this method were described by Bressi et  
196 al. (2014) and Waked et al. (2014). Briefly, PSCF analysis is normally used to identify  
197 possible source areas of pollutants, such as ozone,  $NO_x$  and VOCs. PSCF calculates  
198 the probability that a source is located at latitude  $i$  and longitude  $j$  as:

$$199 \quad PSCF_{ij} = \frac{m_{ij}}{n_{ij}} \quad (1)$$

200 Where  $n_{ij}$  is the number of times that the trajectories passed through the cell  $(i, j)$   
201 and  $m_{ij}$  is the number of times that a source concentration was high when the



202 trajectories passed through the cell (i, j) (Song et al., 2019a). In order to reduce the  
203 uncertainty caused by decreasing small  $n_{ij}$  value, a  $W_{ij}$  function was used in this study  
204 as calculated by Eq. (2):

$$205 \quad W_{ij} = \begin{cases} 1.0, & 3n_{ave} < n_{ij} \\ 0.7, & 1.5n_{ave} < n_{ij} \leq 3n_{ave} \\ 0.4, & 1.0n_{ave} < n_{ij} \leq 1.5n_{ave} \\ 0.2, & n_{ij} \leq n_{ave} \end{cases} \quad (2)$$

206 In this study, the PSCF model were calculated by applying the TrajStat plugins  
207 on MeteInfoMap software version 1.4.4. The 48-h backward trajectories arriving at  
208 Zhengzhou with a trajectory height of 200 m were calculated every hour (00:00–23:00  
209 local time). The studied domain was in the range of 15° to 65° N and 85° to 145° E in  
210 a grid of 0.1° × 0.1° cells, which contains almost all regions overlaid with entire  
211 airflow transport pathways.

## 212 **2.5 Calculation of O<sub>3</sub> formation potential**

213 To understand the impact of the VOC species on ozone formation, Ozone  
214 formation potential (OFP) was used, by using the following equation (Carter, 2010):

$$215 \quad OFP_i = [VOC]_i \times MIR_i \quad (3)$$

216 Where  $[VOC]_i$  is the mass concentration of each VOC, with units of mg/m<sup>3</sup>, MIR  
217 means maximum incremental reactivity (g O<sub>3</sub>/g VOC), and the MIR value of each  
218 VOC is obtained from Carter (1994).



## 219 2.6 Health risk assessment

220 The risk assessment derived from the guidelines proposed by USEPA (2009)  
221 was used to evaluate the adverse health effects of each identified VOC in ambient air  
222 to human health, and evaluate the impact of emission reduction on health risks. In this  
223 paper, the carcinogenic and non-carcinogenic risks were calculated to assess the  
224 impacts of VOCs on human health, by using the Eqs. (4)-(7).

$$225 \quad Risk = IUR \times EC \quad (4)$$

$$226 \quad EC = (CA \times ET \times EF \times ED) / AT \quad (5)$$

$$227 \quad HQ = EC / (RfC \times 1000) \quad (6)$$

$$228 \quad HI = \sum HQ_i \quad (7)$$

229 Where IUR is the estimated unit risk value ( $\text{m}^3/\mu\text{g}$ ); EC is the exposure  
230 concentration ( $\mu\text{g}/\text{m}^3$ ); CA is the environmental concentration ( $\mu\text{g}/\text{m}^3$ ); ET is the  
231 exposure time (h/d); EF is the exposure frequency (d/y); ED is the exposure time (y);  
232 AT is the average time (h); RfC is the reference concentration ( $\text{mg}/\text{m}^3$ ); and HQ is the  
233 non-cancer inhalation hazard quotient and HI is the hazard index. Risk probability  
234 values, including RfC and IUR, were obtained through the risk model calculator  
235 established by the University of Tennessee (RAIS, 2016) and are listed in Table S3.

236 Out of all measured species in this paper, only 46 VOC species with known  
237 toxicity values were considered, including 44 noncarcinogenic species and 21



238 carcinogenic species. Target VOCs and associated toxicity values of health risk  
239 assessment are presented in the Supplementary Materials (Table S4).

## 240 **3. Results and discussion**

### 241 **3.1 Overall observations**

#### 242 **3.1.1 Characteristics of O<sub>3</sub> and other pollution gases**

243 Fig. 1 shows the temporal trends of the O<sub>3</sub> and other pollutant mixing ratios  
244 during the sampling period. During the pre-NMG period, the highest O<sub>3</sub> hourly  
245 concentration was 252 µg/m<sup>3</sup> in 15:00 LST on August 23, meanwhile the max 8-h O<sub>3</sub>  
246 value also appeared on this day (219 µg/m<sup>3</sup>). In addition, max 8-h O<sub>3</sub> concentrations  
247 presented in a total of 7 days, exceeding the ambient air quality standard (GB  
248 3095-2012) Grade II standard of 160 µg/m<sup>3</sup>. At this stage, the ozone pollution cause  
249 concern as the days exceeding the standard accounted for 50%. The highest hourly  
250 concentration of VOCs and NO<sub>x</sub> were 238 ppbv and 357 µg/m<sup>3</sup>, with a mean  
251 concentration of 39 ppbv and 49 µg/m<sup>3</sup> respectively. Higher O<sub>3</sub> precursor  
252 concentrations were observed, which maybe an important factor leading to serious  
253 photochemistry pollution.

254 During the control period, the O<sub>3</sub> precursor concentrations decreased significantly,  
255 with a mean concentration of 34 ppbv VOCs and 39 µg/m<sup>3</sup> NO<sub>x</sub>. However, the ozone  
256 pollution has not been dramatically alleviated; and mild and moderate O<sub>3</sub> pollution  
257 levels accounted for 52% and 10% respectively during the NMG period according to  
258 GB 3095-2012. The phenomenon has been reported that photochemistry is still severe



259 under emergency emission-reduction strategies (Li et al., 2019b). Due to the highly  
260 nonlinear relationships between ozone and its precursors, it is not straightforward to  
261 mitigate ozone pollution by reducing the emissions of VOCs and NO<sub>x</sub> (Tan et al.,  
262 2018; Wang et al., 2019c). A special phenomenon needs to be pointed out that the  
263 ozone concentration during the evening peak is much higher than that in the pre-NMG  
264 period. The weak titrate effect may be the main reason for the phenomena above (Chi  
265 et al., 2018; Zou et al., 2019). At the end of control, the concentration of precursors  
266 increased rapidly, and NO<sub>x</sub> concentration increased by nearly 1.6 times compared  
267 with the control stage. At the same time, the ozone pollution was still severe, the  
268 proportions of mild and moderate pollution days were 83% and 8%, respectively.

269 On the whole, the concentration of ozone precursors decreased significantly  
270 during the control period, and the ozone pollution was severe during the entire  
271 observation period. It should be noted that the maximum value of max 8-h O<sub>3</sub>  
272 concentrations in the NMG period is high of 235 μg/m<sup>3</sup>.

### 273 **3.1.2 Meteorological conditions**

274 Meteorological conditions can significantly influence pollutant concentrations,  
275 which makes it difficult to evaluate the emission reduction brought by emission  
276 control. In this paper, the meteorological data throughout the three periods in  
277 Zhengzhou were compared, including temperature (T), precipitation, relative  
278 humidity (RH), wind speed (WS) and visibility. As shown in Table S5, the  
279 meteorological parameters rarely changed during the three periods (T, 27.4±1.2,



280 24.2±3.3, and 22.3±1.5°C for pre-, during, and post-control periods respectively;  
281 visibility, 16.7±5.5, 14.1±7.0 and 13.0±2.7 km; WS, 1.7±0.3, 1.7±0.4, and 1.5±0.3  
282 m/s). However, the precipitation during pre-control period (236.9 mm) was much  
283 higher than those during control (39.8 mm) and post-control periods (1.6 mm). In  
284 addition, the RH in first stage is higher, which is beneficial to the air pollutants  
285 dissolving in water vapor, condensation and settlement, and then reducing the  
286 concentration of pollutants.

287 Meteorological conditions can influence the transmission and circulation of  
288 regional air pollutants (Ren et al., 2019). In this paper, the air clusters were analyzed  
289 by using the Hybrid Single Particle Lagrangian Integrated Trajectory model to  
290 distinguish the differences of potential source contributions in the three periods. In  
291 previous studies, regional transport has an important influence on Zhengzhou's air  
292 quality, especially the air mass from the BTH region (Jiang et al., 2019; Wang et al.,  
293 2019b). Fig. S4 shows the 48-h backward trajectories results during the sampling  
294 period. The dominant trajectory was from the east or southeast of Zhengzhou in the  
295 three periods. For the pre- and post-NMG periods, Zhengzhou is greatly affected by  
296 the air mass from BTH region, where contained high concentrations of air pollutants  
297 from anthropogenic emissions. Based on the PSCF results in Fig. 2, the high PSCF  
298 values for pollutants (including O<sub>3</sub>, NO<sub>2</sub> and VOCs) were distributed significantly at  
299 the southeast of Zhengzhou and near the Zhengzhou area. Therefore, the potential  
300 source regions for pollutants during the sampling period were mainly from the  
301 southeast of Zhengzhou and local sources within the city. For the record, high PSCF



302 values also presented within northern Hebei Province during the pre-NMG period,  
303 where the region is the major industrialized areas in the BTH. To summarize, in  
304 addition to air pollution control measures, changes of meteorological conditions may  
305 contribute to the improvement of air quality during the NMG period.

### 306 **3.2 Characteristic of VOCs during the three periods**

#### 307 **3.2.1 Mixing ratios and chemical speciation**

308 As illustrated in Fig. 2, the mixing ratios of hourly total VOCs (TVOCs) show  
309 average value of 39 ppbv, ranging from 13 ppbv to 121 ppbv, before the control  
310 period. During control, this was reduced to average of 34 ppbv, with the range from  
311 12 to 78 ppbv. After the control period, the averaged VOC concentration increased to  
312 39 ppbv. Overall, it is clear that the emission control policies were beneficial to  
313 reduce VOC concentration, and reduced by about 16% before and after emission  
314 reduction.

315 The percentage distributions of VOC groups were similar in the three sampling  
316 periods (Fig. S5). Alkanes were the dominant group, accounting 38, 41, and 37% of  
317 the total VOC concentration for three periods respectively, followed by halocarbons.  
318 Notably, OVOCs slightly decreased in the entire sampling period, comprising 17, 16,  
319 and 14%, respectively. However, the active components of aromatics and alkenes  
320 increased over time. Meteorological conditions and the differences in certain  
321 emissions might be key factors that can influence VOC compositions.

322 The top 20 VOC species are summarized in Table 1. The top 20 substances were





323 similar in the three stages, but the concentration levels were quite different. Tracers of  
324 solvent sources including hexane and dichloromethane (Huang and Hsieh, 2019; Wei  
325 et al., 2019) decreased in the control period, chopped by 42% and 47% respectively.  
326 The reduction of vinyl acetate and tetrachloroethylene is relatively large, which may  
327 be attributed to industrial emission reduction (Hsu et al., 2018; Zhang et al., 2015). In  
328 addition, the concentration of acetylene is reduced by 55% compared with the  
329 pre-NMG period, as a potential result of the control of combustion sources (Liu et al.,  
330 2020; Wu et al., 2016a). However, isoprene, a tracer of biogenic VOCs (Kumar et al.,  
331 2018), decreased over time, which was mainly attributed to the meteorological  
332 conditions.

### 333 **3.2.2 Diurnal variations of ambient VOCs**

334 The mean diurnal variations of TVOC and their compounds before, during, and  
335 after the control period are shown in Fig. S6. Clearly, the diurnal variations of TVOCs  
336 during the three periods are similar, showing higher values from evening till morning  
337 rush hours while lowest in the afternoon. The composition of alkanes, alkenes,  
338 alkynes and aromatics shows similar daily variations. Previous studies have  
339 suggested that VOCs can be oxidized by O<sub>3</sub>, OH radicals and NO<sub>3</sub> radicals (Song et  
340 al., 2019b). In short, the reactions with O<sub>3</sub> and OH radicals are the most important  
341 chemical reactions during daytime, and the reactions with NO<sub>3</sub> radicals and O<sub>3</sub> are  
342 dominant reactions for VOCs occurring at night (Atkinson and Arey, 2003). However,  
343 the reaction rate of the OH radical is much higher than that of the NO<sub>3</sub> radical, and  
344 thus, the concentration of TVOC and its compounds at night is generally higher than



345 that during the daytime (Atkinson and Arey, 2003). It should be noted that the average  
346 VOC mixing ratio at midnight during the control period was significantly lower than  
347 that in other two period, especially the concentrations of aromatics and halogenated  
348 compounds were significantly decreased.

349 As each source type has its own fingerprint, the mean diurnal variations of  
350 tracers during the three periods are presented in Fig. 3. *n*-pentanes at the three  
351 periods have several minor peaks (e.g., 02:00 and 18:30 LST). The 02:00 LST peak  
352 is mainly from the freight trucks and the 7:00 LST peak is most likely from traffic  
353 rush-hour emissions (Li et al., 2019c). It should be noted that during the control  
354 period, the nighttime concentration significantly decreased while the daytime  
355 concentrations of the three stages are close. Toluene, ethylbenzene, and xylenes (Fig.  
356 3) as well as the tracer gas of NO and NO<sub>2</sub> (Fig. S7) at the three periods had similar  
357 diurnal patterns to those of pentane. All of the species mentioned above are tracers of  
358 traffic emission (Yang et al., 2018). It is speculated that the control effect on muck  
359 truck is significant during the control period. As shown in Fig. 3, tracers of solvent  
360 utilization, such as hexane, dichloromethane, had different diurnal patterns to those  
361 of vehicle source. During the pre-NMG period, the solvent tracer emissions are so  
362 strong that they almost offset the daytime valley caused by photochemical reaction  
363 and boundary layer height (Li et al., 2019c). The daytime levels of the NMG period  
364 are lower than those of first stage, which might attribute to the intensive control over  
365 the use of outdoor solvents. Chloromethane and acetylene are tracers of biomass



366 burning and combustion, respectively (Hui et al., 2019). During control period,  
367 acetylene decreased significantly, while chloromethane remained higher levels.

### 368 **3.3 Source attribution and apportionment**

#### 369 **3.3.1 Ratios of specific compounds**

370 During the sampling period, the great changes in the mixing ratios of VOCs may  
371 be caused by the altered contribution of emission sources. Ratios of specific VOCs  
372 has commonly been used to identify emission sources.

373 Because *i*- and *n*-pentane have similar atmospheric lifetimes, these *i/n* ratios are  
374 widely used to examine the impact of vehicle emissions to combustion emissions and  
375 the values varied according to sources (i.e., 0.56-0.80 for coal combustion, 1.5-3.0 for  
376 liquid gasoline, 2.2-3.8 for vehicle emissions (Yan et al., 2017; Zheng et al., 2018).  
377 Isopentane and *n*-pentane showed highly significant correlations during the three  
378 periods ( $R^2 > 0.6$ ), suggesting the source of these two species was similar (Fig. S8). In  
379 this study, the ratios of *i/n*-pentane during the three periods were 1.5, 1.7 and 1.5,  
380 indicating that the VOCs originated from the mixed sources of coal combustion and  
381 vehicle emissions.

382 The toluene/benzene (T/B) ratio has also been widely applied to be indicator of  
383 sources. A previous study reported that these two species are most probably from  
384 biomass burning, coal combustion, vehicle emissions and solvent used, when the T/B  
385 ratios ranging between 0.2-0.6, 0.6-1.0, 1.0-2.0 and  $> 4$ , respectively (Hui et al., 2018;  
386 Kumar et al., 2018; Song et al., 2019b). As shown in Fig. S8, low correlations ( $R^2 =$



387 0.3-0.5) were found during the three period, suggesting a more complex set of sources  
388 for the two species. The T/B ratio among the three period was 0.78, 0.75 and 0.92,  
389 respectively, indicating that the VOCs were greatly influenced by the mixed source of  
390 coal combustion and vehicle emissions. The ratio was lower in the control period.  
391 Acetylene concentration was low but the chloromethane concentration was high  
392 during the control period, indicating biomass burning had a greater impact during the  
393 period.

### 394 **3.3.2 Identification of PMF factors**

395 The 42 most abundant species, accounted for almost 90% total VOC  
396 concentrations, were selected to apply in the PMF receptor model to analyze the  
397 relative contribution of each potential source. The factor profiles of seven emission  
398 sources, namely, liquefied petroleum gas (LPG) evaporation, industrial processes,  
399 vehicle exhausts, biomass burning, biogenic source, solvent usage and coal  
400 combustion, were identified in Fig. 4.

401 Source 1 was characterized by both high proportions and high abundances of  
402 ethane (38%), ethene (53%), propane (43%) and other C<sub>3</sub>-C<sub>5</sub> alkanes. A high  
403 proportion of short linear alkanes, such as ethane and propane, was likely released  
404 from the use of LPG (Yadav et al., 2019; Zhang et al., 2015). Consequently factor 1  
405 was assigned to LPG.

406 Source 2 accounts for larger percentages of carbon disulfide and  
407 halohydrocarbon, such as *cis*-1,2-dichloroethylene, chlorotrifluoromethane,



408 trichloromethane, dichloromethane, 1,2-dichloroethane, 1,2-dichloropropane,  
409 followed by some aromatics. Some previous study indicated that these species were  
410 related to industrial process (Hui et al., 2020; Zhang et al., 2018). Furthermore,  
411 ethylene, considered as the blood of the development in industry (Song et al., 2019a;  
412 Zheng et al., 2020), accounted of almost 65% of the TVOCs in this factor. Therefore,  
413 this source is considered to be related to industrial processes.

414 Source 3 was characterized by a high percentage of some C<sub>4</sub>-C<sub>5</sub> alkanes and  
415 aromatics. Toluene, ethyl-benzene, *m,p*-xylene, *o*-xylene, *i,n*-butane and *i,n*-pentane  
416 are all associated with vehicle exhausts (Huang and Hsieh, 2019; Liu et al., 2019).  
417 Furthermore, the T/B ratio was approximate 1.6, suggesting that this source was  
418 significantly affected by vehicle exhaust emissions. Factor 3 also includes high  
419 proportions of methyl tert-butyl ether, which is a common gasoline additive in China  
420 (Yang et al., 2018). Therefore, this factor can be labeled as vehicle exhaust.

421 Source 4 has high concentrations of chloromethane, which is a typical tracer of  
422 biomass burning (Ling et al., 2011; Zhang et al., 2019). The percentages of benzene  
423 and toluene were lower, but they could still not be neglected, and the T/B ratio was <  
424 0.5 (Li et al., 2019a). Thus, source 4 was identified as biomass burning.

425 Source 5 accounts for larger percentages of isoprene, accounting for 86% of the  
426 TVOCs in the source. Isoprene is an indicator of biogenic emissions and emits from  
427 many plants (Hui et al., 2018; Song et al., 2019a). This factor also included a  
428 considerable proportion of intermediate products (Liu et al., 2019), such as acetone,



429 2-hexanone and 2-butanone. Therefore, this source is considered to be biogenic  
430 emissions.

431 Source 6 was differentiated by C<sub>6</sub>-C<sub>8</sub> alkanes, such as *n*-hexane, methyl  
432 cyclopentane, 3-methylpentane, 2-methylpentane and 2,3-dimethylbutane. The  
433 percentages of ethyl acetate, tetrachloroethylene, carbon tetrachloride, chloroform,  
434 dichloromethane were high. Those substances are important organic solvents, and  
435 typical tracers of solvent usage (Hui et al., 2018, 2020). Meanwhile, there are virtually  
436 no other short chain hydrocarbon in this source. Therefore, source 6 was primarily  
437 attributed to solvent usage rather than industrial processes or vehicle emission source.

438 Source 7 was dominated by acetylene, which accounted for 75% of the TVOCs  
439 in the source. Acetylene is a typical tracer of combustion emission (Hui et al., 2019;  
440 Wu et al., 2016b). Some of the VOC species, such as alkanes and benzene, are the  
441 main components in emissions from coal burning (Liu et al., 2019; Song et al., 2019b.,  
442 Yang et al., 2018). Thus, factor 7 was assigned to combustion emission.

### 443 3.3.3 Contributions of VOC sources

444 The concentrations of hourly mixing ratio and the relative contributions of each  
445 VOC sources are illustrated in Fig. 5. Compared with the non-control periods, the  
446 contributions of coal combustion, vehicle exhausts and solvent utilization are  
447 significantly reduced during the control period.

448 Conversely, the mixing ratios of LPG showed higher values during the control  
449 period. Peak values of biomass combustion presented frequently during the second



450 period, and biomass combustion accounts for a relatively high proportion in this stage.  
451 The highest concentration was observed in the afternoon of the 18<sup>th</sup> of September.  
452 Zhengzhou and its surrounding areas are in the harvest period of crops in September,  
453 so the emissions of biomass combustion need to be concerned. Fig. S9 shows the  
454 hotspots diagram of Zhengzhou and its surrounding areas during the observation  
455 period, and the number of fire spots in September was significantly higher than that in  
456 August.

457 Time series of each identified source contributions are shown in Fig. 6. During  
458 the first period, solvent utilization ( $33 \mu\text{g}/\text{m}^3$ ) was the largest contributor and  
459 accounted for 30% of TVOCs, followed by industrial process ( $26 \mu\text{g}/\text{m}^3$ , 24%) and  
460 vehicle exhausts ( $24 \mu\text{g}/\text{m}^3$ , 22%). Although it was not the heating time, coal  
461 combustion still accounted 10% of the TVOCs, probably due to several coal-fired  
462 power plants around Zhengzhou (Li et al., 2019a). In contrast, the proportion of  
463 biomass combustion was very low during this period, accounting for only 2% of the  
464 TVOCs.

465 During the control period, solvent utilization and industrial process made the  
466 largest contribution (23%) to atmospheric VOCs, with the concentration of  $23 \mu\text{g}/\text{m}^3$ ,  
467 followed by vehicle emissions (22%) and LPG (11%). Biomass burning should not be  
468 ignored in this period, accounting for 10% of total VOCs. The contribution from coal  
469 combustion was relatively low ( $3.5 \mu\text{g}/\text{m}^3$ ), accounting only for 4% of TVOCs.



470 For the third period, the largest contributor was fuel combustion related to  
471 vehicle exhausts, with  $30 \mu\text{g}/\text{m}^3$ , accounting for 28% of total VOCs. Industrial  
472 processes ( $23 \mu\text{g}/\text{m}^3$ ), solvent utilization ( $20 \mu\text{g}/\text{m}^3$ ), biomass burning ( $12 \mu\text{g}/\text{m}^3$ ), coal  
473 combustion ( $11 \mu\text{g}/\text{m}^3$ ), LPG ( $5.7 \mu\text{g}/\text{m}^3$ ) and biogenic emissions ( $5.6 \mu\text{g}/\text{m}^3$ )  
474 accounting for 21, 19, 11, 10, 5 and 5% of total VOCs, respectively.

475 In summary, the concentrations of solvent utilization were reduced to the greatest  
476 extent during the control period, with the value of  $10 \mu\text{g}/\text{m}^3$  in the pre-NMG period,  
477 followed by coal combustion ( $7.1 \mu\text{g}/\text{m}^3$ ), industrial processes ( $4.0 \mu\text{g}/\text{m}^3$ ) and vehicle  
478 exhausts ( $2.2 \mu\text{g}/\text{m}^3$ ). Reductions of solvent utilization, coal combustion, industrial  
479 processes and vehicle exhausts were responsible for 80, 57, 32 and 18% of the  
480 reductions in ambient VOCs, indicating that the control measures on solvent  
481 utilization and coal combustion were the most effective. In contrast, due to weak  
482 control on biomass burning and LPG, contributions from these sources were elevated  
483 by 66 and 28 %, respectively. September is a harvest month in northern China, which  
484 means that biomass burning contributions might increase with time. Meanwhile, the  
485 peak contribution of this source occurred during the control period, because of a lack  
486 of relative control measures for LPG.

### 487 **3.4 Atmospheric environmental implications**

488 In this section, the atmospheric environmental implications of VOCs were  
489 discussed by calculating the values of ozone formation potential (OFP) and risk  
490 assessment.





### 491 **3.4.1 Variations of OFP**

492 The OFP and their compositions during the three periods are shown in Fig. S10.  
493 The total OFP during the control period was  $183 \mu\text{g}/\text{m}^3$ , which was 0.77 and 0.83  
494 times lower than those before and after control period, respectively. As shown in Fig.  
495 S10, the aromatics were the dominant contributors to total OFP in all three periods,  
496 comprising 42, 50 and 56 %, respectively, followed by OVOCs, alkanes, alkenes,  
497 halohydrocarbon and acetylene. Aromatics played a key role in ozone formation,  
498 which is similar to many previous reports (Huang and Hsieh, 2019; Song et al., 2019a;  
499 Yang et al., 2019b).

500 The source contributions to OFP were calculated by PMF model (Table 2). The  
501 most important source to ozone formation was traffic emissions. Industrial emissions  
502 and solvent usage were the second and third sources of photochemical ozone  
503 formation. Among them, solvent use has the greatest contribution to the OFP  
504 reduction with the emission reduction during the control period, explaining the 48 %  
505 reduction in OFP. Although combustion contributes only 10% of the total OFP, this  
506 source played an important role in the reduction in OFP, explaining the 33% to the  
507 OFP reduction. At the same time, control of traffic and industry also reduced the OFP  
508 during the games. Thus, solvent utilization and combustion controls were the most  
509 important measures taken to reduce OFP during National Minority Games 2019 in  
510 Zhengzhou. However, the current knowledge about formation mechanisms of  $\text{O}_3$  is  
511 still very limited, and the next section discuss the sensitivity of ozone.



### 512 **3.4.2 Risk assessment of individual VOC species**

513 In addition to the impacts on ambient air quality, some VOC species are also  
514 toxic with various health impacts. In this paper, the non-carcinogenic risk (expressed  
515 by HQ) and carcinogenic risk (expressed by lifetime cancer risk, LCR) of hazardous  
516 VOC species were investigated, and the acceptable safety threshold were 1 and  
517  $1 \times 10^{-6}$ , respectively (USEPA, 2009). On the whole, the HQ of almost substances is  
518 far below the safety threshold, indicating no chance of non-carcinogenic risk.  
519 However, only the HQ of acrolein (1.8) exceeded the value of 1, suggesting obvious  
520 chance of non-carcinogenic effects (Fig. 7). As for LCR, six species were above  
521  $1 \times 10^{-6}$  in this study, including 1,2-dichloroethane ( $2.5 \times 10^{-5}$ ), chloroform ( $1.1 \times 10^{-5}$ ),  
522 1,2-dibromoethane ( $8.1 \times 10^{-6}$ ), naphthalene ( $6.4 \times 10^{-6}$ ), benzene ( $5.2 \times 10^{-6}$ ) and  
523 tetrachloromethane ( $3.3 \times 10^{-6}$ ).

524 During the entire observation period, a total of seven VOCs may pose potential  
525 risks to the human health. Health risk assessment in Zhengzhou was compared with  
526 other cities, as shown in Table S3. Overall, the values of risk assessment in this study  
527 are evidently lower than those reported in Beijing (Gu et al., 2019) and Langfang  
528 (Yang et al., 2019a), whereas higher than the summer of 2018 in Zhengzhou (Li et al.,  
529 2020). Evaluated health risk assessment before, during, and after the control period  
530 shows cumulative LCR was  $5.8 \times 10^{-5}$ ,  $5.1 \times 10^{-5}$  and  $6.3 \times 10^{-5}$  respectively during the  
531 three periods (Fig. S11). Control measures can reduce non-carcinogenic risk. On the  
532 other hand, values of six substances still exceed the acceptable safety threshold of  
533 LCR during the control period. As for non-carcinogenic risk assessment, the HI was



534 1.6, 2.1 and 2.1, respectively. Noticeably, the HQ of acrolein (1.9) during the control  
535 period was higher than the other two periods, which should be paid more attention. In  
536 summary, VOC concentrations decreased significantly during the control period, but  
537 still posed health risks to humans. Therefore, we need to focus on the targeted  
538 emission reduction of these characteristic substances to protect human health.

### 539 **3.5 O<sub>3</sub>-NO<sub>x</sub>-VOCs sensitivity and control strategies**

540 The impact of ozone precursors on ozone formation can be described as either a  
541 NO<sub>x</sub>-limited or VOCs-limited regime, which is an important step in developing  
542 effective control strategies to reduce regional ozone pollution. The ratios of  
543 VOCs/NO<sub>x</sub> have been widely used to determine the ozone formation regime.  
544 Generally, VOCs-sensitive regimes occur when VOCs/NO<sub>x</sub> ratios are lower than 10  
545 (ppb C/ppb); ozone formation to be NO<sub>x</sub>-limited when the ratios are greater than  
546 20.(Li et al., 2019a, 2021; Sillman, 1999 ).

547 The diurnal variations of the VOCs/NO<sub>x</sub> ratios before, during, and after the  
548 control period are shown in Fig. 8, and the ratios for the three periods showed similar  
549 daily variations. Higher ratios were observed at midnight (1:00-6:00), especially  
550 during the control period (Fig. 8) due to the emission reduction of NO<sub>x</sub> emissions,  
551 with the VOCs/NO<sub>x</sub> ratios of 10. Afterwards, the ratio decreased rapidly, indicating  
552 that NO<sub>x</sub> concentration increased faster than NMHCs due to the effect of vehicular  
553 emissions (Zou et al., 2019). Thereafter, the ratio of VOC/NO<sub>x</sub> also increased with  
554 the continuous accumulation of O<sub>3</sub> concentration.



555 At the peak time of O<sub>3</sub> concentration (12:00-16:00), the average VOCs/NO<sub>x</sub>  
556 ratio was approximately 9.3 during the pre-NMG period, which was slightly lower  
557 than 10 and thus proved that the ozone generation in this period was limited by VOCs.  
558 During the control period, the ratio in the afternoon was lower than that in the  
559 pre-NMG period, with a mean value of 7.1. In this study, the mean values of  
560 VOCs/NO<sub>x</sub> (ppbv C/ppbv) were below 10 during all three periods, indicating that the  
561 O<sub>3</sub> formation was sensitive to VOCs in Zhengzhou, and the reductions of the VOC  
562 emissions will be beneficial for O<sub>3</sub> alleviation.

563 It should be noted that ozone sensitivity can only be initially determined by the  
564 VOCs/NO<sub>x</sub> ratio, and the next part it will be verified by WRF-CMAQ model.

565 The CMAQ developed by USEPA was used to simulate the ozone pollution  
566 processes in Zhengzhou in August and September 2019. The sensitivity of emission  
567 sources to ozone pollution in Zhengzhou was analyzed by using source sensitivity  
568 identification tool DDM-3d (Hakami et al., 2004). As shown in Fig 9, the values of  
569 sensitivity\_NO<sub>x</sub>/sensitivity\_VOCs were generally lower than 0.8 in the urban district  
570 of Zhengzhou and its surrounding areas, while the ratio of the western part of  
571 Zhengzhou is more than 1.2. Thus, O<sub>3</sub> formation is quite sensitive to VOCs, and that  
572 means VOCs should be controlled in priority to the effect control of O<sub>3</sub>. To achieve a  
573 more effective reduction, it is necessary to study reduction ratio that has the greatest  
574 effect on control strategies in reducing ozone concentration.

575 The EKMA of O<sub>3</sub>-VOC-NO<sub>x</sub> sensitivity analysis is presented in Fig. 10. The



576 results reflect that cutting VOCs can alleviate ozone pollution, while reducing NO<sub>x</sub>  
577 concentration might lead to the increase of ozone concentration. Some scholars have  
578 pointed out that the reaction rate constant between NO<sub>x</sub> and OH radical is 5.5 times  
579 higher than that of VOCs and OH radical (Chen et al., 2019). Therefore, the reduction  
580 of NO<sub>x</sub> may lead to increase OH radicals from the VOC oxidation cycle thereby  
581 promoting the formation of O<sub>3</sub>. Response of ozone to its precursors (VOCs and NO<sub>x</sub>)  
582 under different emission reduction scenarios are shown in Fig. 10. Reduction of ozone  
583 precursors will not improve photochemical pollution when reduction ratios of the  
584 precursors (VOC:NO<sub>x</sub>) is less than 1. As shown in Fig. 10, O<sub>3</sub> levels decreased most  
585 effectively for the only VOC reduction scheme with VOCs: NO<sub>x</sub> = 2:1 (using mol  
586 ratio). It should be noted that it is nearly impossible to reduce VOC emissions only  
587 while NO<sub>x</sub> remains unchanged, because VOCs (particularly anthropogenic VOCs)  
588 and NO<sub>x</sub> are generally co-emitted (Chen et al., 2019).

589 During the NMG period, the government has carried out stringent emission  
590 controls. The concentrations of ozone precursors showed a decreasing trend, but the  
591 ozone pollution was still serious. Unreasonable emission reduction may be an  
592 important factor leading to ozone pollution. Combined with the results of this study, it  
593 is suggested that reduction ratios of the precursors (VOCs:NO<sub>x</sub>) should be more than  
594 2 to effectively alleviate ozone pollution. Controlling VOC sources is the key to  
595 alleviate the local ozone pollution, especially the control of aromatic hydrocarbons.  
596 The solvent usage are non-combustion processes, and therefore reducing VOC  
597 emission from this source will not contribute to the decrease of NO<sub>x</sub> emission. This



598 finding could guide the formulation and implementation of effective O<sub>3</sub> control

599 strategies in Zhengzhou.

600



## 601 **4. Conclusions**

602 A number of strict emission control measures were implemented in Zhengzhou  
603 and its surrounding area to ensure good air quality during NMG period. The  
604 concentrations of VOCs and NO<sub>x</sub> decreased significantly; however, O<sub>3</sub> pollution has  
605 not been effectively alleviated. To provide scientific references and guidance for  
606 atmospheric control strategies, this study systematically quantified the impacts of  
607 characterizing level, photochemical reactivity, source contribution of the VOCs and  
608 the ozone-NO<sub>x</sub>-VOC sensitivities during sporting events in Zhengzhou.

609 The mixing ratios of TVOCs during control period was 34 ppbv, and cut down  
610 by about 16% than those before and after emission reduction. Source apportioning  
611 showed that solvent usage, industrial processes, vehicle exhausts, LPG, biomass  
612 burning, biogenic source and coal combustion were the major sources of VOCs, and  
613 the seven sources accounting for 23%, 23%, 22%, 11%, 10%, 7% and 4% during the  
614 MNG period. The control measures on solvent utilization and coal combustion were  
615 most effective, accounting for 80 and 57% of the reductions in ambient VOCs,  
616 respectively. However, contributions of biomass burning were elevated. The total OFP  
617 during the control period was 183 µg/m<sup>3</sup>, which was 0.23 and 0.17 times lower than  
618 those before and after control period, respectively. Measurements on solvent  
619 utilization and combustion were the most important controls to reduce OFP during  
620 NMG period.

621 The O<sub>3</sub>-NO<sub>x</sub>-VOC sensitivity showed that Zhengzhou is under VOC-sensitive



622 regimes. Cutting VOCs can alleviate ozone pollution, while excessively reducing  
623 NO<sub>x</sub> concentration might lead to the increase of ozone concentration. Unreasonable  
624 emission reduction may aggravate ozone pollution during control periods. It is  
625 suggested that emission reduction ratios of the precursors (VOC:NO<sub>x</sub>) should be  
626 more than 2. Considering that the solvent usage are non-combustion processes,  
627 reducing VOC emission from this sources will not cause the decrease of NO<sub>x</sub>  
628 emission, therefore the solvent source can be controlled preferentially.

629





630 **Data availability**

631 The data set is available to the community and can be accessed by request from

632 Ruiqin Zhang (rqzhang@zzu.edu.cn).

633

634



## 635 **Author contribution**

636       YSJ and ZRQ planned and organized the study, and were deeply involved in  
637 writing the manuscript. SFC, YSS and WSB performed the atmospheric  
638 measurements and data analysis and wrote the manuscript. HB, FXG and YMH  
639 assisted heavily with the atmospheric measurements and data analysis. SFC and XRX  
640 conducted the model development and data analysis.

641       Other coauthors provided useful insights in data analysis and contributed to the  
642 writing of the manuscript.

643       YSJ and SFC contributed equally to this work.

644



## 645 **Acknowledgments**

646        This work was supported by the Study of Collaborative Control of PM<sub>2.5</sub> and  
647 O<sub>3</sub> Pollution in Zhengzhou City (No. 20200321A) and National Key Research and  
648 Development Program of China (No. 2017YFC0212403).

649

650



## 651 **References**

- 652 Atkinson, R., Arey, J., 2003. Atmospheric degradation of volatile organic compounds.  
653 Chem. Rev. 103, 4605–4638.
- 654 Bai, L., Lu, X., Yin, S., Zhang, H., Ma, S., Wang, C., Li, Y., Zhang, R., 2020. A  
655 recent emission inventory of multiple air pollutant, PM<sub>2.5</sub> chemical species and  
656 its spatial-temporal characteristics in central China. J. Clean. Prod. 269, 112-114.
- 657 Baudic, A., Gros, V., Sauvage, S., Locoge, N., Sanchez, O., Sarda-Estève, R.,  
658 Kalogridis, C., Petit, J.-E., Bonnaire, N., Baisnée, D., Favez, O., Albinet, A.,  
659 Sciare, J., Bonsang, B., 2016. Seasonal variability and source apportionment of  
660 volatile organic compounds (VOCs) in the Paris megacity (France). Atmos.  
661 Chem. Phys. 16, 11961-11989.
- 662 Bressi, M., Sciare, J., Ghersi, V., Mihalopoulos, N., Petit, J.E., Nicolas, J.B.,  
663 Moukhtar, S., Rosso, A., Feron, A., Bonnaire, N., Poulakis, E., Theodosi, C.,  
664 2014. Sources and geographical origins of fine aerosols in Paris (France). Atmos.  
665 Chem. Phys. 14, 8813–8839.
- 666 Carter, W.P.L., 1994. Development of ozone reactivity scales for volatile organic  
667 compounds. J. Air Waste Manag. Assoc. 44, 881–899.
- 668 Carter, W.P.L., 2010. Updated maximum incremental reactivity scale and  
669 hydrocarbon bin reactivities for regulatory applications. Prep. Calif. Air Resour.  
670 Board Contract. 07-339.
- 671 Chan, K.L., Hartl, A., Lam, Y.F., Xie, P.H., Liu, W.Q., Cheung, H.M., Lampel, J.,  
672 Pöhler, D., Li, A., Xu, J., Zhou, H.J., Ning, Z., Wenig, M.O., 2015. Observations



673 of tropospheric NO<sub>2</sub> using ground based MAX-DOAS and OMI measurements  
674 during the Shanghai World Expo 2010. *Atmos. Environ.* 119, 45-58.

675 Chen, X., Situ, S., Zhang, Q., Wang, X., Sha, C., Zhou, L., Wu, L., Wu, L., Ye, L.,  
676 Li, C., 2019. The synergetic control of NO<sub>2</sub> and O<sub>3</sub> concentrations in a  
677 manufacturing city of southern China. *Atmos. Environ.* 201, 402-416.

678 Chi, X., Liu, C., Xie, Z., Fan, G., Wang, Y., He, P., Fan, S., Hong, Q., Wang, Z., Yu,  
679 X., Yue, F., Duan, J., Zhang, P., Liu, J., 2018. Observations of ozone vertical  
680 profiles and corresponding precursors in the low troposphere in Beijing, China.  
681 *Atmos. Res.* 213, 224-235.

682 Gu, Y., Li, Q., Wei, D., Gao, L., Tan, L., Su, G., Liu, G., Liu, W., Li, C., Wang, Q.,  
683 2019. Emission characteristics of 99 NMVOCs in different seasonal days and the  
684 relationship with air quality parameters in Beijing, China. *Ecotoxicol. Environ.*  
685 *Saf.* 169, 797-806.

686 Hakami, A.; Henze, D. K.; Seinfeld, J. H.; Singh, K.; Sandu, A.; Kim, S.; Byun, D.;  
687 Li, Q., 2007. The adjoint of CMAQ. *Environ. Sci. Technol.* 41, 7807-7817.

688 Hsu, C.Y., Chiang, H.C., Shie, R.H., Ku, C.H., Lin, T.Y., Chen, M.J., Chen, N.T.,  
689 Chen, Y.C., 2018. Ambient VOCs in residential areas near a large-scale  
690 petrochemical complex: Spatiotemporal variation, source apportionment and  
691 health risk. *Environ. Pollut.* 240, 95-104.

692 Hu, R., Liu, G., Zhang, H., Xue, H., Wang, X., 2018. Levels, characteristics and  
693 health risk assessment of VOCs in different functional zones of Hefei.  
694 *Ecotoxicol. Environ. Saf.* 160, 301-307.



- 695 Huang, W., Fang, D., Shang, J., Li, Z., Zhang, Y., Huo, P., Liu, Z., Schauer, J.J.,  
696 Zhang, Y., 2018. Relative impact of short-term emissions controls on gas and  
697 particle-phase oxidative potential during the 2015 China Victory Day Parade in  
698 Beijing, China. *Atmos. Environ.* 183, 49-56.
- 699 Huang, Y.S., Hsieh, C.C., 2019. Ambient volatile organic compound presence in the  
700 highly urbanized city: source apportionment and emission position. *Atmos.*  
701 *Environ.* 206, 45-59.
- 702 Hui, L., Liu, X., Tan, Q., Feng, M., An, J., Qu, Y., Zhang, Y., Cheng, N., 2019. VOC  
703 characteristics, sources and contributions to SOA formation during haze events  
704 in Wuhan, Central China. *Sci. Total. Environ.* 650, 2624-2639.
- 705 Hui, L., Liu, X., Tan, Q., Feng, M., An, J., Qu, Y., Zhang, Y., Deng, Y., Zhai, R.,  
706 Wang, Z., 2020. VOC characteristics, chemical reactivity and sources in urban  
707 Wuhan, central China. *Atmos. Environ.* 224, 117340.
- 708 Hui, L., Liu, X., Tan, Q., Feng, M., An, J., Qu, Y., Zhang, Y., Jiang, M., 2018.  
709 Characteristics, source apportionment and contribution of VOCs to ozone  
710 formation in Wuhan, Central China. *Atmos. Environ.* 192, 55-71.
- 711 Jaars, K., Vestenius, M., van Zyl, P.G., Beukes, J.P., Hellén, H., Vakkari, V., Venter,  
712 M., Josipovic, M., Hakola, H., 2018. Receptor modelling and risk assessment of  
713 volatile organic compounds measured at a regional background site in South  
714 Africa. *Atmos. Environ.* 172, 133-148.
- 715 Jiang, N., Li, L., Wang, S., Li, Q., Dong, Z., Duan, S., Zhang, R., Li, S., 2019.  
716 Variation tendency of pollution characterization, sources, and health risks of



- 717 PM<sub>2.5</sub>-bound polycyclic aromatic hydrocarbons in an emerging megacity in  
718 China: Based on three-year data. *Atmos. Res.* 217, 81-92.
- 719 Kumar, A., Singh, D., Kumar, K., Singh, B.B., Jain, V.K., 2018. Distribution of  
720 VOCs in urban and rural atmospheres of subtropical India: Temporal variation,  
721 source attribution, ratios, OFP and risk assessment. *Sci. Total. Environ.* 613-614,  
722 492-501.
- 723 Li, B.W., Ho, S.S.H., Gong, S.L., Ni, J.W., Li, H.R., Han, L.Y., Yang, Y., Qi, Y.J.,  
724 Zhao, D.X., 2019a. Characterization of VOCs and their related atmospheric  
725 processes in a central Chinese city during severe ozone pollution periods. *Atmos.*  
726 *Chem. Phys.* 19, 617-638.
- 727 Li, H., Wang, D., Cui, L., Gao, Y., Huo, J., Wang, X., Zhang, Z., Tan, Y., Huang, Y.,  
728 Cao, J., Chow, J.C., Lee, S.C., Fu, Q., 2019b. Characteristics of atmospheric  
729 PM<sub>2.5</sub> composition during the implementation of stringent pollution control  
730 measures in shanghai for the 2016 G20 summit. *Sci. Total. Environ.* 648,  
731 1121-1129.
- 732 Li, J., Xie, S.D., Zeng, L.M., Li, L.Y., Li, Y.Q., Wu, R.R., 2015. Characterization of  
733 ambient volatile organic compounds and their sources in Beijing, before, during,  
734 and after Asia-Pacific Economic Cooperation China 2014. *Atmos. Chem. Phys.*  
735 15, 7945-7959.
- 736 Li, J., Zhai, C., Yu, J., Liu, R., Li, Y., Zeng, L., Xie, S., 2018. Spatiotemporal  
737 variations of ambient volatile organic compounds and their sources in Chongqing,  
738 a mountainous megacity in China. *Sci. Total. Environ.* 627, 1442-1452.



- 739 Li, K., Li, J., Tong, S., Wang, W., Huang, R.-J., Ge, M., 2019c. Characteristics of  
740 wintertime VOCs in suburban and urban Beijing: concentrations, emission ratios,  
741 and festival effects. *Atmos. Chem. Phys.* 19, 8021-8036.
- 742 Li, K., Li, J., Wang, W., Tong, S., Liggio, J., Ge, M., 2017. Evaluating the  
743 effectiveness of joint emission control policies on the reduction of ambient  
744 VOCs: Implications from observation during the 2014 APEC summit in  
745 suburban Beijing. *Atmos. Environ.* 164, 117-127.
- 746 Li, R., Wang, Z., Cui, L., Fu, H., Zhang, L., Kong, L., Chen, W., Chen, J., 2019d. Air  
747 pollution characteristics in China during 2015-2016: Spatiotemporal variations  
748 and key meteorological factors. *Sci. Total. Environ.* 648, 902-915.
- 749 Li, Y., Yin, S., Yu, S., Bai, L., Wang, X., Lu, X., Ma, S., 2021. Characteristics of  
750 ozone pollution and the sensitivity to precursors during early summer in central  
751 plain, China. *J. Environ. Sci. (in China)*. 99, 354-368.
- 752 Li, Y., Yin, S., Yu, S., Yuan, M., Dong, Z., Zhang, D., Yang, L., Zhang, R., 2020.  
753 Characteristics, source apportionment and health risks of ambient VOCs during  
754 high ozone period at an urban site in central plain, China. *Chemosphere* 250,  
755 126283.
- 756 Ling, Z.H., Guo, H., Cheng, H.R., Yu, Y.F., 2011. Sources of ambient volatile  
757 organic compounds and their contributions to photochemical ozone formation at  
758 a site in the Pearl River Delta, southern China. *Environ. Pollut.* 159, 2310-2319.
- 759 Liu, Y., Song, M., Liu, X., Zhang, Y., Hui, L., Kong, L., Zhang, Y., Zhang, C., Qu, Y.,  
760 An, J., Ma, D., Tan, Q., Feng, M., 2020. Characterization and sources of volatile





761 organic compounds (VOCs) and their related changes during ozone pollution  
762 days in 2016 in Beijing, China. *Environ. Pollut.* 257, 113599.

763 Liu, Y., Wang, H., Jing, S., Gao, Y., Peng, Y., Lou, S., Cheng, T., Tao, S., Li, L., Li,  
764 Y., Huang, D., Wang, Q., An, J., 2019. Characteristics and sources of volatile  
765 organic compounds (VOCs) in Shanghai during summer: Implications of  
766 regional transport. *Atmos. Environ.* 215, 116902.

767 Ma, T., Duan, F., He, K., Qin, Y., Tong, D., Geng, G., Liu, X., Li, H., Yang, S., Ye,  
768 S., Xu, B., Zhang, Q., Ma, Y., 2019. Air pollution characteristics and their  
769 relationship with emissions and meteorology in the Yangtze River Delta region  
770 during 2014-2016. *J. Environ. Sci. (in China)*. 83, 8-20.

771 Norris, G., Duvall, R., Brown, S., Bai, S., 2014. EPA Positive Matrix Factorization  
772 (PMF) 5.0. Fundamentals and User Guide. US Environmental Protection Agency,  
773 EPA/600/R-14/108, Washington, DC.

774 RAIS (The Risk Assessment Information System), 2009. [http://rais.ornl.gov/tools/  
775 profile.php](http://rais.ornl.gov/tools/profile.php).

776 Ren, Y., Li, H., Meng, F., Wang, G., Zhang, H., Yang, T., Li, W., Ji, Y., Bi, F., Wang,  
777 X., 2019. Impact of emission controls on air quality in Beijing during the 2015  
778 China Victory Day Parade: Implication from organic aerosols. *Atmos. Environ.*  
779 198, 207-214.

780 Schleicher, N., Norra, S., Chen, Y., 2012. Efficiency of mitigation measures to reduce  
781 particulate air pollution-a case study during the Olympic Summer Games 2008 in  
782 Beijing, China. *Sci. Total. Environ.* 427-428, 146-158.



- 783 Sillman, S., 1999. The relation between ozone, NO<sub>x</sub> and hydrocarbons in urban and  
784 polluted rural environments. *Atmos. Environ.* 33, 1821–1845.
- 785 Song, C., Liu, B., Dai, Q., Li, H., Mao, H., 2019a. Temperature dependence and  
786 source apportionment of volatile organic compounds (VOCs) at an urban site on  
787 the north China plain. *Atmos. Environ.* 207, 167-181.
- 788 Song, M., Liu, X., Zhang, Y., Shao, M., Lu, K., Tan, Q., Feng, M., Qu, Y., 2019b.  
789 Sources and abatement mechanisms of VOCs in southern China. *Atmos. Environ.*  
790 201, 28-40.
- 791 Su, F., Xu, Q., Wang, K., Yin, S., Wang, S., Zhang, R., Tang, X., Ying, Q., 2021. On  
792 the effectiveness of short-term intensive emission controls on ozone and  
793 particulate matter in a heavily polluted megacity in central China. *Atmos.*  
794 *Environ.* 246, 118111.
- 795 Tan, Z., Lu, K., Dong, H., Hu, M., Li, X., Liu, Y., Lu, S., Shao, M., Su, R., Wang, H.,  
796 Wu, Y., Wahner, A., Zhang, Y., 2018. Explicit diagnosis of the local ozone  
797 production rate and the ozone-NO<sub>x</sub>-VOC sensitivities. *Sci. Bull.* 63, 1067-1076.
- 798 Ulbrich, I., Canagaratna, M., Zhang, Q., Worsnop, D., Jimenez, J., 2009.  
799 Interpretation of organic components from Positive Matrix Factorization of  
800 aerosol mass spectrometric data. *Atmos. Chem. Phys.* 9, 2891–2918.
- 801 USEPA, 2009. Risk Assessment Guidance for Superfund Volume I: Human Health  
802 Evaluation Manual (Part F, Supplemental Guidance for Inhalation Risk  
803 Assessment). EPA-540-R-070–002. US Environmental Protection Agency,  
804 Washington, DC, USA.



- 805 Waked, A., Favez, O., Alleman, L.Y., Piot, C., Petit, J.E., Delaunay, T., Verlinden, E.,  
806 Golly, B., Besombes, J.L., Jaffrezo, J.L., Leoz-Garziandia, E., 2014. Source  
807 apportionment of PM<sub>10</sub> in a north-western Europe regional urban background site  
808 (Lens, France) using positive matrix factorization and including primary  
809 biogenic emissions. *Atmos. Chem. Phys.* 14, 3325–3346.
- 810 Wang, M., Zhu, T., Zheng, J., Zhang, R.Y., Zhang, S.Q., Xie, X.X., 2009. Use of a  
811 mobile laboratory to evaluate changes in on-road air pollutants during the  
812 Beijing 2008 Summer Olympics. *Atmos. Chem. Phys.* 9, 8247–8263.
- 813 Wang, N., Lyu, X., Deng, X., Huang, X., Jiang, F., Ding, A., 2019c. Aggravating O<sub>3</sub>  
814 pollution due to NO<sub>x</sub> emission control in eastern China. *Sci. Total. Environ.* 677,  
815 732-744.
- 816 Wang, P., Chen, Y., Hu, J., Zhang, H., Ying, Q., 2019a. Attribution of tropospheric  
817 ozone to NO<sub>x</sub> and VOC emissions: considering ozone formation in the transition  
818 regime. *Environ. Sci. Technol.* 53, 1404-1412.
- 819 Wang, S., He, B., Yuan, M., Su, F., Yin, S., Yan, Q., Jiang, N., Zhang, R., Tang, X.,  
820 2019b. Characterization of individual particles and meteorological conditions  
821 during the cold season in Zhengzhou using a single particle aerosol mass  
822 spectrometer. *Atmos. Res.* 219, 13-23.
- 823 Wang, W., Jing, L., Zhan, J., Wang, B., Zhang, D.P., Zhang, H.W., Wang, D.Q.,  
824 Yang, Y., Zhao, J., Sun, Y.F., Bi, X.H., Wang, X.T., Feng, J.L., 2014. Nitrated  
825 polycyclic aromatic hydrocarbon pollution during the Shanghai World Expo  
826 2010. *Atmos. Environ.* 89, 242-248.



- 827 Wei, X.-Y., Liu, M., Yang, J., Du, W.-N., Sun, X., Huang, Y.-P., Zhang, X., Khalil,  
828 S.K., Luo, D.-M., Zhou, Y.-D., 2019. Characterization of PM<sub>2.5</sub>-bound PAHs and  
829 carbonaceous aerosols during three-month severe haze episode in Shanghai,  
830 China: Chemical composition, source apportionment and long-range  
831 transportation. *Atmos. Environ.* 203, 1-9.
- 832 Wu, F., Yu, Y., Sun, J., Zhang, J., Wang, J., Tang, G., Wang, Y., 2016a.  
833 Characteristics, source apportionment and reactivity of ambient volatile organic  
834 compounds at Dinghu Mountain in Guangdong Province, China. *Sci. Total.  
835 Environ.* 548-549, 347-359.
- 836 Wu, R., Li, J., Hao, Y., Li, Y., Zeng, L., Xie, S., 2016b. Evolution process and  
837 sources of ambient volatile organic compounds during a severe haze event in  
838 Beijing, China. *Sci. Total. Environ.* 560-561, 62-72.
- 839 Xiong, Y., Du, K., 2020. Source-resolved attribution of ground-level ozone formation  
840 potential from VOC emissions in Metropolitan Vancouver, BC. *Sci. Total.  
841 Environ.* 721, 137698.
- 842 Xu, W., Liu, X., Liu, L., Dore, A.J., Tang, A., Lu, L., Wu, Q., Zhang, Y., Hao, T., Pan,  
843 Y., Chen, J., Zhang, F., 2019. Impact of emission controls on air quality in  
844 Beijing during APEC 2014: Implications from water-soluble ions and  
845 carbonaceous aerosol in PM<sub>2.5</sub> and their precursors. *Atmos. Environ.* 210,  
846 241-252.
- 847 Yadav, R., Sahu, L.K., Tripathi, N., Pal, D., Beig, G., Jaaffrey, S.N.A., 2019.  
848 Investigation of emission characteristics of NMVOCs over urban site of western



- 849 India. *Environ. Pollut.* 252, 245-255.
- 850 Yan, Y., Peng, L., Li, R., Li, Y., Li, L., Bai, H., 2017. Concentration, ozone formation  
851 potential and source analysis of volatile organic compounds (VOCs) in a thermal  
852 power station centralized area: A study in Shuozhou, China. *Environ. Pollut.* 223,  
853 295-304.
- 854 Yang, W., Zhang, Y., Wang, X., Li, S., Zhu, M., Yu, Q., Li, G., Huang, Z., Zhang, H.,  
855 Wu, Z., Song, W., Tan, J., Shao, M., 2018. Volatile organic compounds at a rural  
856 site in Beijing: influence of temporary emission control and wintertime heating.  
857 *Atmos. Chem. Phys.* 18, 12663-12682.
- 858 Yang, Y., Ji, D., Sun, J., Wang, Y., Yao, D., Zhao, S., Yu, X., Zeng, L., Zhang, R.,  
859 Zhang, H., Wang, Y., Wang, Y., 2019a. Ambient volatile organic compounds in  
860 a suburban site between Beijing and Tianjin: Concentration levels, source  
861 apportionment and health risk assessment. *Sci. Total. Environ.* 695, 133889.
- 862 Yang, Y., Liu, X., Zheng, J., Tan, Q., Feng, M., Qu, Y., An, J., Cheng, N., 2019b.  
863 Characteristics of one-year observation of VOCs, NO<sub>x</sub>, and O<sub>3</sub> at an urban site in  
864 Wuhan, China. *J. Environ. Sci. (in China)*. 79, 297-310.
- 865 Yenisoy-Karakas, S., Dorter, M., Odabasi, M., 2020. Intraday and interday variations  
866 of 69 volatile organic compounds (BVOCs and AVOCs) and their source  
867 profiles at a semi-urban site. *Sci. Total. Environ.* 723, 138028.
- 868 Yu, S., Yin, S., Zhang, R., Wang, L., Su, F., Zhang, Y., Yang, J., 2020.  
869 Spatiotemporal characterization and regional contributions of O<sub>3</sub> and NO<sub>2</sub>: An  
870 investigation of two years of monitoring data in Henan, China. *J. Environ. Sci.*



- 871 (in China). 90, 29-40.
- 872 Zeng, P., Lyu, X.P., Guo, H., Cheng, H.R., Jiang, F., Pan, W.Z., Wang, Z.W., Liang,  
873 S.W., Hu, Y.Q., 2018. Causes of ozone pollution in summer in Wuhan, Central  
874 China. *Environ. Pollut.* 241, 852-861.
- 875 Zhang, H., Chen, G., Hu, J., Chen, S., Wiedinmyer, C., Kleeman, M., Ying, Q., 2014.  
876 Evaluation of a seven-year air quality simulation using the Weather Research  
877 and Forecasting (WRF)/Community Multiscale Air Quality (CMAQ) models in  
878 the eastern United States. *Sci. Total. Environ.* 473-474, 275-85.
- 879 Zhang, Y., Hong, Z., Chen, J., Xu, L., Hong, Y., Li, M., Hao, H., Chen, Y., Qiu, Y.,  
880 Wu, X., Li, J.-R., Tong, L., Xiao, H., 2020. Impact of control measures and  
881 typhoon weather on characteristics and formation of PM<sub>2.5</sub> during the 2016 G20  
882 summit in China. *Atmos. Environ.* 224, 233-248.
- 883 Zhang, Y., Li, R., Fu, H., Zhou, D., Chen, J., 2018. Observation and analysis of  
884 atmospheric volatile organic compounds in a typical petrochemical area in  
885 Yangtze River Delta, China. *J. Environ. Sci. (in China)*. 71, 117312.
- 886 Zhang, Y., Sun, J., Zheng, P., Chen, T., Liu, Y., Han, G., Simpson, I.J., Wang, X.,  
887 Blake, D.R., Li, Z., Yang, X., Qi, Y., Wang, Q., Wang, W., Xue, L., 2019.  
888 Observations of C1-C5 alkyl nitrates in the Yellow River Delta, northern China:  
889 Effects of biomass burning and oil field emissions. *Sci. Total. Environ.* 656,  
890 129-139.
- 891 Zhang, Y., Wang, X., Zhang, Z., Lu, S., Huang, Z., Li, L., 2015. Sources of C(2)-C(4)  
892 alkenes, the most important ozone nonmethane hydrocarbon precursors in the



893 Pearl River Delta region. *Sci. Total. Environ.* 502, 236-245.

894 Zheng, H., Kong, S., Xing, X., Mao, Y., Hu, T., Ding, Y., Li, G., Liu, D., Li, S., Qi,  
895 S., 2018. Monitoring of volatile organic compounds (VOCs) from an oil and gas  
896 station in northwest China for 1 year. *Atmos. Chem. Phys.* 18, 4567-4595.

897 Zheng, H., Kong, S., Yan, Y., Chen, N., Yao, L., Liu, X., Wu, F., Cheng, Y., Niu, Z.,  
898 Zheng, S., Zeng, X., Yan, Q., Wu, J., Zheng, M., Liu, D., Zhao, D., Qi, S., 2020.  
899 Compositions, sources and health risks of ambient volatile organic compounds  
900 (VOCs) at a petrochemical industrial park along the Yangtze River. *Sci. Total.*  
901 *Environ.* 703, 135505.

902 Zou, Y., Charlesworth, E., Yin, C.Q., Yan, X.L., Deng, X.J., Li, F., 2019. The  
903 weekday/weekend ozone differences induced by the emissions change during  
904 summer and autumn in Guangzhou, China. *Atmos. Environ.* 199, 114-126.

905



## Figure list

**Fig. 1** Time series of VOCs and trace gases during the sampling period in Zhengzhou.

**Fig. 2** The average weighted PSCF maps for O<sub>3</sub>, NO<sub>2</sub> and VOCs in Zhengzhou during the three periods.

**Fig. 3** Diurnal variations in concentrations of some reactive VOC species in Zhengzhou during the three periods.

**Fig. 4** Source profiles calculated using the PMF model.

**Fig. 5** Time series of each identified source contributions and accumulated relative VOC contributions.

**Fig. 6** Source contributions to VOCs concentration in the PMF model during the three period.

**Fig. 7** Non-carcinogenic risks of HQ and carcinogenic risks for individual VOC species.

**Fig. 8** Daily variations in the VOC/NO<sub>x</sub> ratio in Zhengzhou before, during, and after NMG periods.

**Fig. 9** Spatial comparison of O<sub>3</sub>-NO<sub>x</sub>-VOCs sensitive regime between August and September 2019 in Zhengzhou.

**Fig. 10** The O<sub>3</sub> isopleth diagram versus NO<sub>x</sub> and VOCs using EKMA (a) and variation chart of O<sub>3</sub> concentration in each control path (b) during pre-NMG period in Zhengzhou.



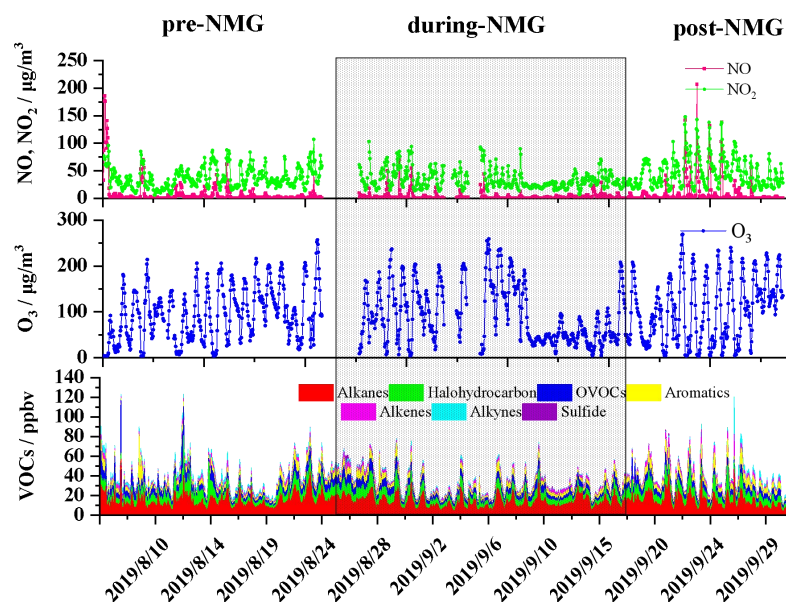


**Fig. 1** Time series of VOCs and trace gases during the sampling period in Zhengzhou.

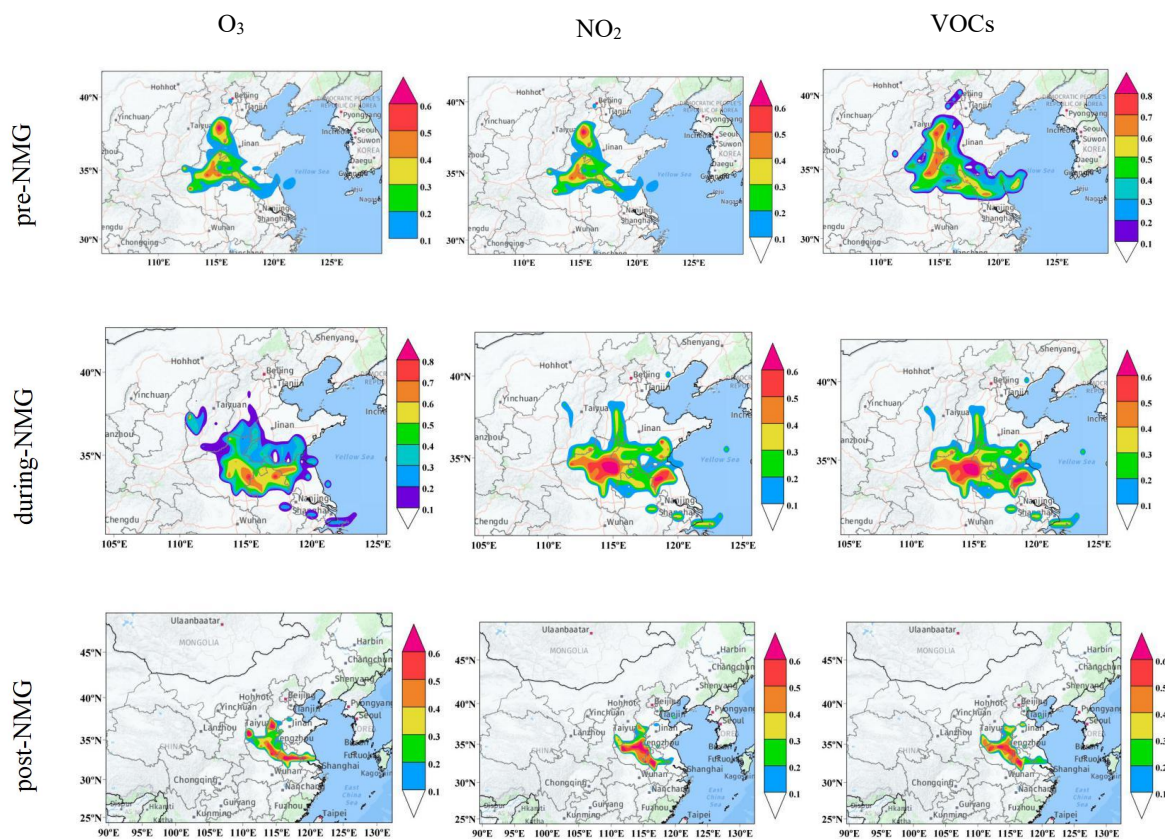


Fig. 2 The average weighted PSCF maps for O<sub>3</sub>, NO<sub>2</sub> and VOCs in Zhengzhou during the three periods.

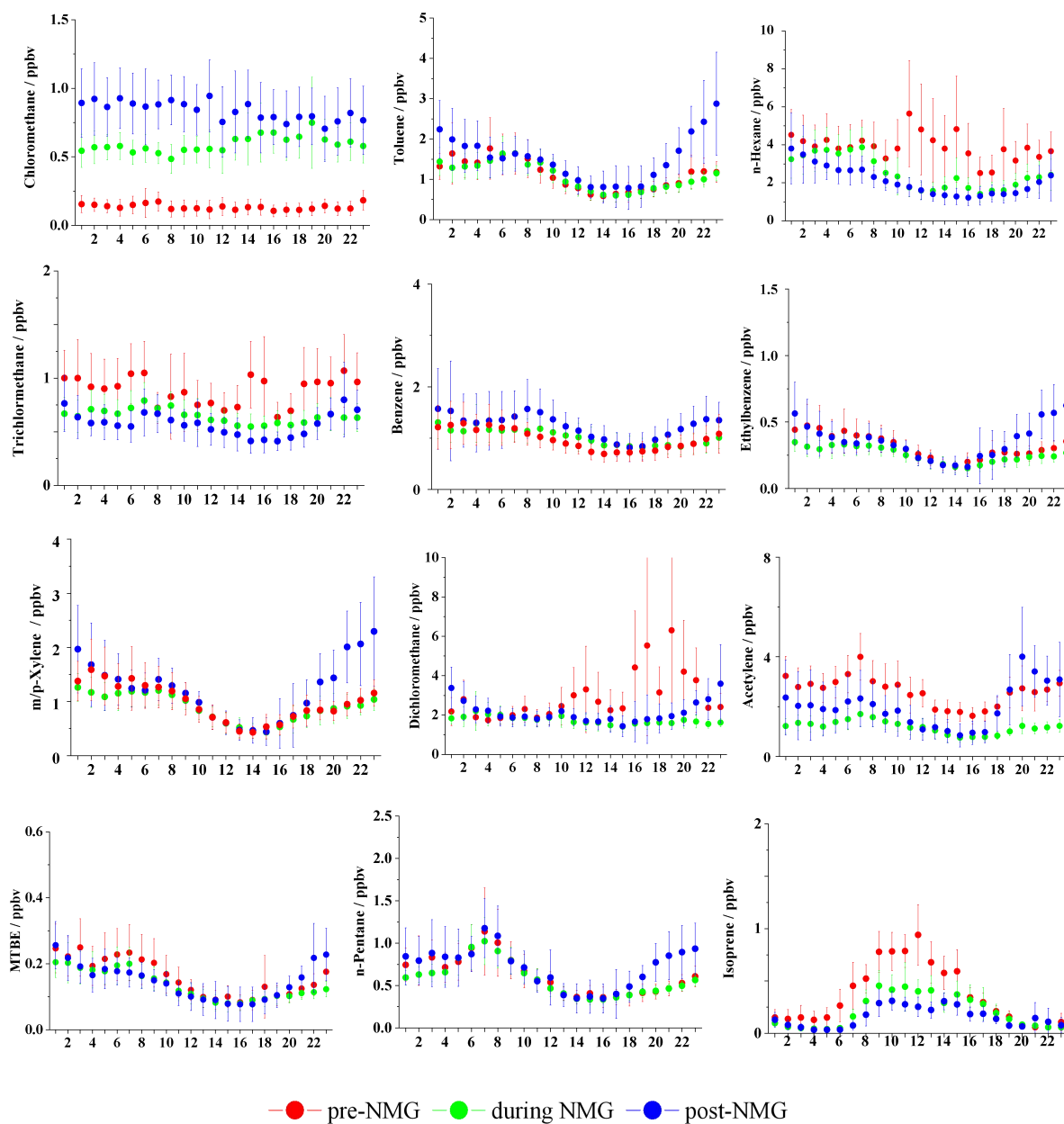


Fig. 3 Diurnal variations in concentrations of some reactive VOC species in Zhengzhou during the three periods.

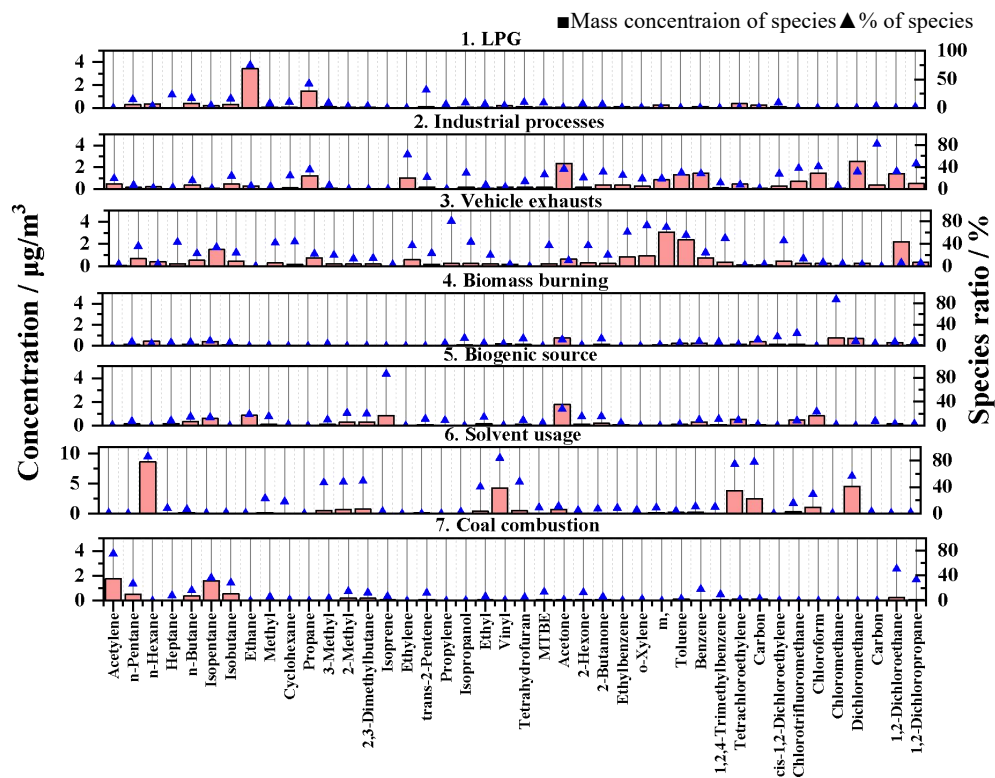


Fig. 4 Source profiles calculated using the PMF model.

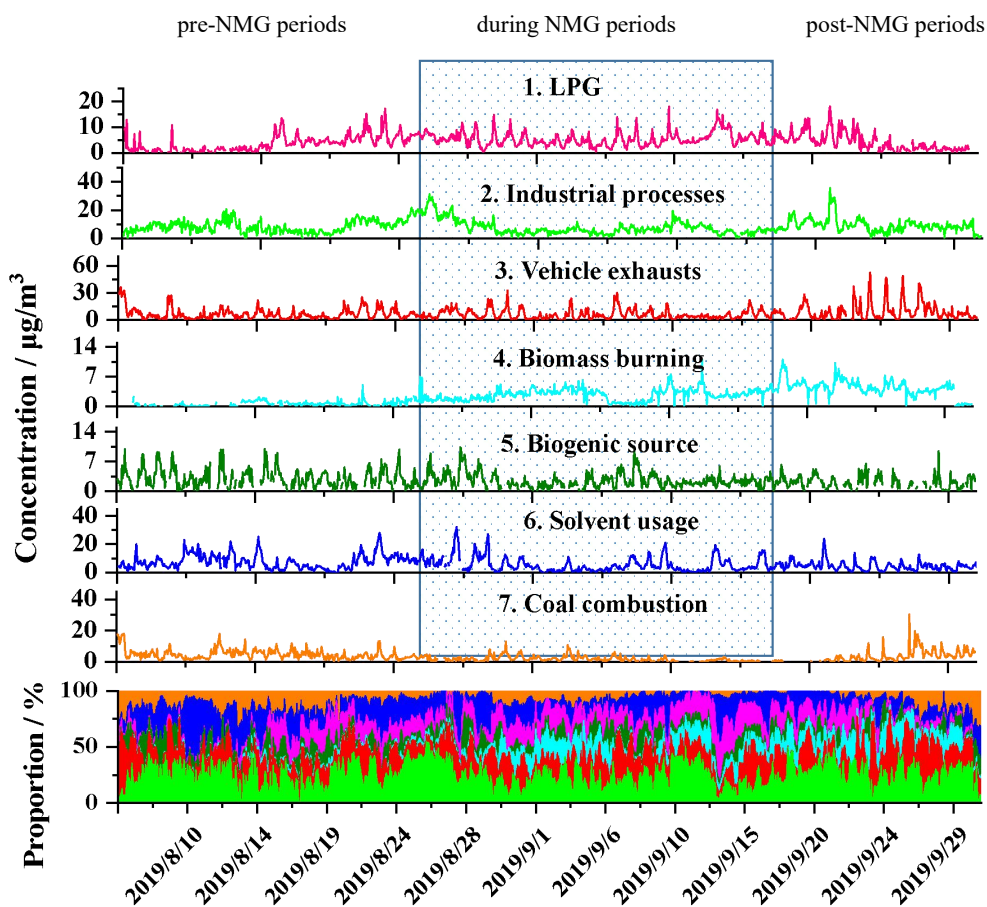
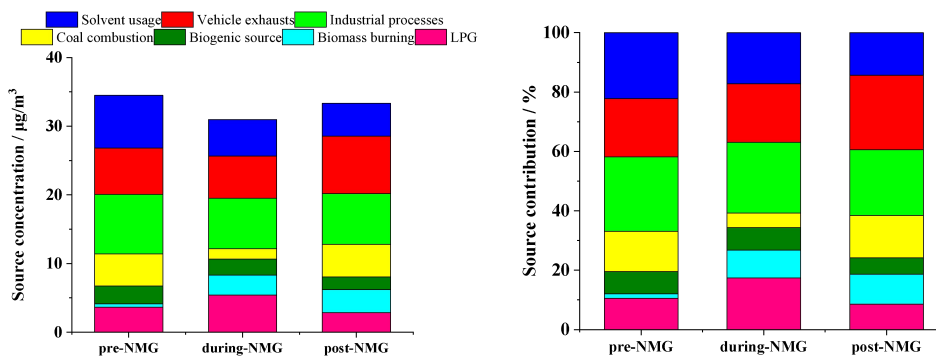


Fig. 5 Time series of each identified source contributions and accumulated relative VOC contributions.



**Fig. 6** Source contributions to VOCs concentration in the PMF model during the three period.

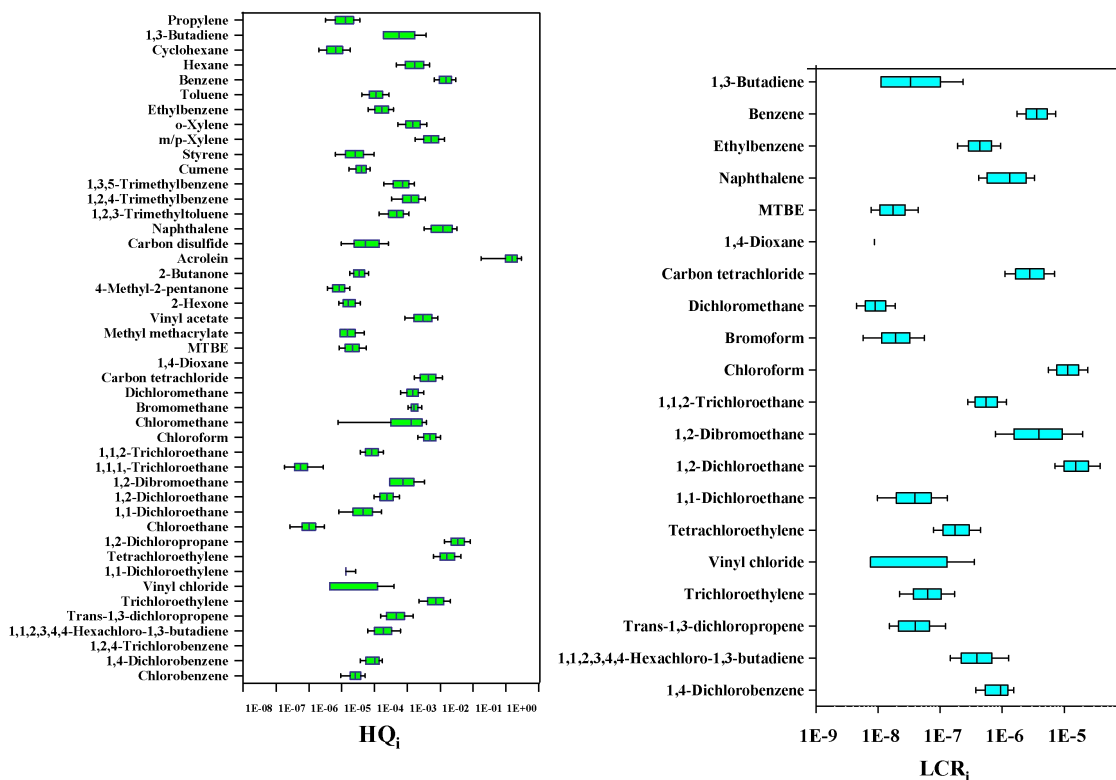
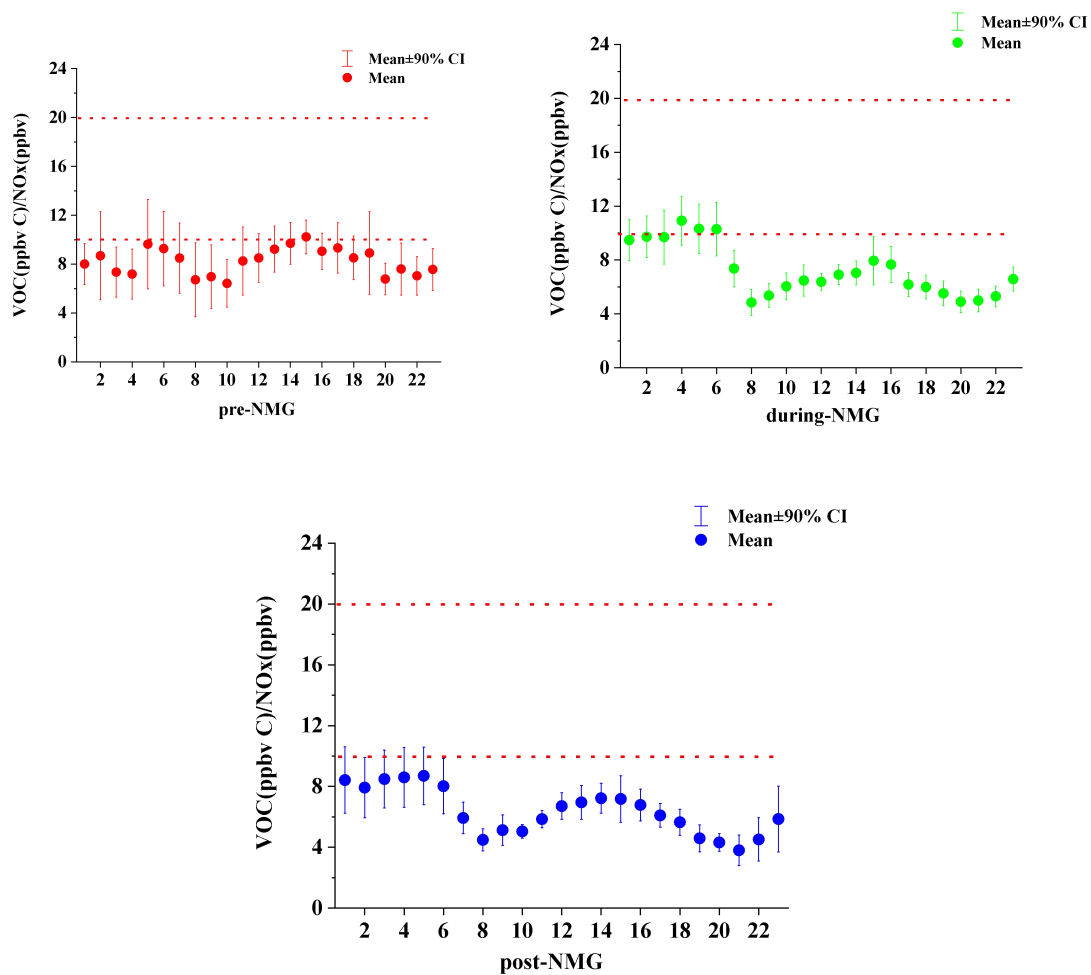
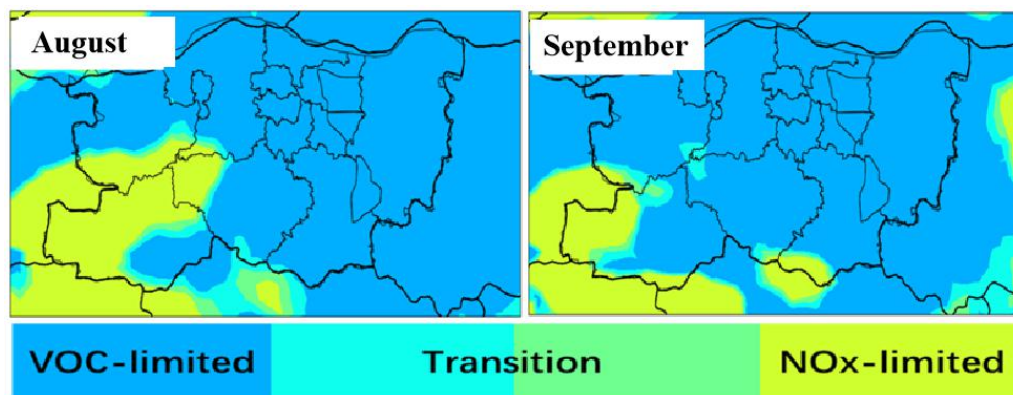


Fig. 7 Non-carcinogenic risks of HQ and carcinogenic risks for individual VOC species.



**Fig. 8** Daily variations in the VOC/NO<sub>x</sub> ratio in Zhengzhou before, during, and after NMG periods.





**Fig. 9** Spatial comparison of  $O_3$ - $NO_x$ -VOCs sensitive regime between August and September 2019 in Zhengzhou.

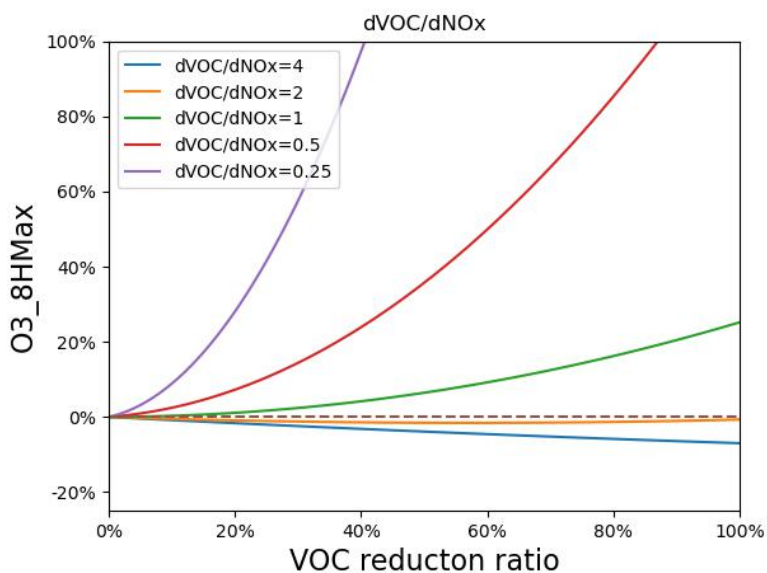
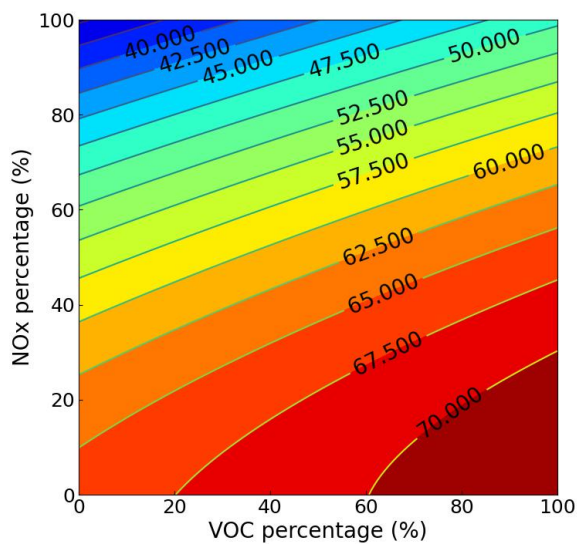


**Fig. 10** The O<sub>3</sub> isopleth diagram versus NO<sub>x</sub> and VOCs using EKMA (a) and variation chart of O<sub>3</sub> concentration in each control path (b) during pre-NMG period in Zhengzhou.



## Table list

**Table 1** Concentrations of the 20 most abundant species in Zhengzhou (unit: ppbv).

**Table 2** OFP contributions ( $\mu\text{g}/\text{cm}^3$ ) of each VOC source during the sampling periods in Zhengzhou.



**Table 1** Concentrations of the 20 most abundant species in Zhengzhou (unit: ppbv).

Component	Before	Component	During	Component	After
n-Hexane	4.3	Ethane	4.2	Ethane	3.2
Dichloromethane	3.3	Acetone	2.5	Acetone	2.7
Ethane	3.1	n-Hexane	2.5	n-Propane	2.6
Acetone	2.9	n-Propane	2.1	Acetylene	2.5
Acetylene	2.6	Dichloromethane	1.8	Dichloromethane	2.2
Vinyl acetate	2.2	Ethylene	1.4	n-Hexane	2.1
n-Propane	1.9	Vinyl acetate	1.3	Ethylene	2
Isopentane	1.4	Acetylene	1.2	Isopentane	1.6
Ethylene	1.2	Isopentane	1.2	Toluene	1.5
Toluene	1.2	Toluene	1.1	1,2-Dichloroethane	1.4
1,2-Dichloroethane	1.1	1,2-Dichloroethane	1.0	Benzene	1.2
Benzene	1.0	Benzene	1.0	m-Xylene	1.2
m-Xylene	1.0	m-Xylene	0.9	n-Butane	1.1
n-Butane	1.0	n-Butane	0.8	Vinyl acetate	1.0
Chloroform	0.9	Isobutane	0.8	Isobutane	1.0
Tetrachloroethylene	0.9	Tetrachloroethylene	0.7	Chloromethane	0.8
Isobutane	0.9	Chloroform	0.7	n-Pentane	0.8
n-Pentane	0.6	carbon tetrachloride	0.6	Chloroform	0.6
Carbon tetrachloride	0.6	Chloromethane	0.6	Tetrachloroethylene	0.6
2-Butanone	0.4	n-Pentane	0.6	Carbon tetrachloride	0.5
$\Sigma$ TOP 20 species / $\Sigma$ VOCs	83%		79%		78%



**Table 2** OFP contributions ( $\mu\text{g}/\text{m}^3$ ) of each VOC source during the sampling periods in Zhengzhou.

Source	Source contribution		
	pre-NMG	during-NMG	post-NMG
LPG	8.7	13	6.9
biomass burning	1.5	8.4	9.8
Biogenic source	18.6	16.6	13.1
coal combustion	14.6	4.8	14.9
industrial processes	41.4	33.3	35.5
vehicle exhausts	72.1	65.3	89
Solvent use	46.2	32.1	28.8
Total	203.1	173.5	198.0